Toxicology and Applied Pharmacology 386 (2020) 114830

Contents lists available at ScienceDirect

Toxicology and Applied Pharmacology

journal homepage: www.elsevier.com/locate/taap

Effects of physicochemical properties of TiO_2 nanomaterials for pulmonary inflammation, acute phase response and alveolar proteinosis in intratracheally exposed mice

Pernille Høgh Danielsen[a], Kristina Bram Knudsen[a], Janez Štrancar[b], Polona Umek[b], Tilen Koklič[b], Maja Garvas[b], Esa Vanhala[c], Sauli Savukoski[c], Yaobo Ding[d], Anne Mette Madsen[a], Nicklas Raun Jacobsen[a], Ingrid Konow Weydahl[a], Trine Berthing[a], Sarah Søs Poulsen[a], Otmar Schmid[d], Henrik Wolff[c,e], Ulla Vogel[a,f,*]

[a] National Research Centre for the Working Environment, Copenhagen Ø, Denmark
[b] Jožef Stefan Institute, Ljubljana, Slovenia
[c] Finnish Institute of Occupational Health, Helsinki, Finland
[d] Institute of Lung Biology and Disease, Helmholtz Zentrum München, German Research Center for Environmental Health, Munich, Germany
[e] Helsinki University, Department of Pathology, Helsinki, Finland
[f] DTU Health Tech, Technical University of Denmark, Kgs. Lyngby, Denmark

ARTICLE INFO

Keywords:
Titanium dioxide
Nanoparticles
Crystal phase
Inflammation
Acute phase response
Pulmonary alveolar proteinosis

ABSTRACT

Nanomaterial (NM) characteristics may affect the pulmonary toxicity and inflammatory response, including specific surface area, size, shape, crystal phase or other surface characteristics. Grouping of TiO_2 in hazard assessment might be challenging because of variation in physicochemical properties. We exposed C57BL/6 J mice to a single dose of four anatase TiO_2 NMs with various sizes and shapes by intratracheal instillation and assessed the pulmonary toxicity 1, 3, 28, 90 or 180 days post-exposure. The quartz DQ12 was included as benchmark particle. Pulmonary responses were evaluated by histopathology, electron microscopy, bronchoalveolar lavage (BAL) fluid cell composition and acute phase response. Genotoxicity was evaluated by DNA strand break levels in BAL cells, lung and liver in the comet assay. Multiple regression analyses were applied to identify specific TiO_2 NMs properties important for the pulmonary inflammation and acute phase response. The TiO_2 NMs induced similar inflammatory responses when surface area was used as dose metrics, although inflammatory and acute phase response was greatest and more persistent for the TiO_2 tube. Similar histopathological changes were observed for the TiO_2 tube and DQ12 including pulmonary alveolar proteinosis indicating profound effects related to the tube shape. Comparison with previously published data on rutile TiO_2 NMs indicated that rutile TiO_2 NMs were more inflammogenic in terms of neutrophil influx than anatase TiO_2 NMs when normalized to total deposited surface area. Overall, the results suggest that specific surface area, crystal phase and shape of TiO_2 NMs are important predictors for the observed pulmonary effects of TiO_2 NMs.

1. Introduction

The global increase in production and application of titanium dioxide nanomaterials (TiO_2 NMs) in a wide range of industrial and consumer products leads to potential exposure-related adverse health effects for workers. In the workplace, exposure is most likely to occur via inhalation and thus cause lung inflammation as well as systemic effects. TiO_2 NMs are poorly soluble and have been considered as low toxicity particles. However, The International Agency for Research on Cancer (IARC) has classified TiO_2 as a Group 2B carcinogen (possibly carcinogenic to humans) based on sufficient evidence in animal experiments (IARC, 2010) as lung tumors developed in rats after two years of chronic exposure to 250 mg/m^3 of fine-sized rutile TiO_2 (Lee et al., 1985) and to 10 mg/m^3 of nano-sized TiO_2 P25 (Heinrich et al., 1995). A large number of rodent studies have reported increased pulmonary inflammation, including neutrophil influx in bronchoalveolar lavage (BAL) fluid, after acute, sub-acute and sub-chronic exposure to TiO_2 NMs by either inhalation or intratracheal (i.t.) instillation (Shi

* Corresponding author at: National Research Centre for the Working Environment, Copenhagen Ø, Denmark.
E-mail address: ubv@nrcwe.dk (U. Vogel).

https://doi.org/10.1016/j.taap.2019.114830
Received 3 October 2019; Received in revised form 12 November 2019; Accepted 14 November 2019
Available online 15 November 2019

et al., 2013; Hadrup et al., 2017). Neutrophil influx in BAL fluid has been shown to correlate closely with pulmonary acute phase response in terms of increased serum amyloid A 3 (*Saa3*) mRNA levels in lung tissue of mice exposed to TiO_2 NMs by i.t. instillation and by inhalation (Halappanavar et al., 2011; Saber et al., 2013). It has been suggested that the SAA produced in the lungs enters systemic circulation as part of high density lipoprotein molecules, causing reversal of the cholesterol flow leading to increased formation of foam cells and plaque progression, and that this contributes significantly to the pathogenesis of cardiovascular disease (Saber et al., 2014). NM characteristics may affect the pulmonary toxicity and inflammatory response, including specific surface area, size, shape, crystal phase, chemical composition, charge or other surface characteristics. The importance of particle size has been discussed widely in the past as the smaller sized NMs and accompanying increased specific surface area entails increased toxicity and translocation, greater lung retention and slower pulmonary clearance (Ferin et al., 1992; Stone et al., 2017). A larger specific surface area provides a larger interface for molecular and chemical interactions with biological fluids and tissues, potentially increasing the reactivity of NMs. Numerous in vivo studies on particle-induced acute pulmonary toxicity in animal models have confirmed that the most biological relevant dose metric for predicting adverse outcomes, such as inflammation, is likely the specific surface area rather than mass, as shown in a retrospective analysis by Schmid & Stoeger (Schmid and Stoeger, 2016). The crystal phase of TiO_2 NMs has likewise been suggested to be important for the toxic response (Johnston et al., 2009), but relatively few studies have investigated this, and with ambiguous results. Grouping of TiO_2 in hazard assessment might be challenging because of the variation in physicochemical properties. In the present study, the TiO_2 NMs are of various sizes and shapes of the anatase crystal phase. We will also compare the results with previous studies on TiO_2 NMs of the rutile crystal phase. The shape of NMs can have an effect on the specific surface area and in some cases, as in case of fibers, it also seems to have a qualitative effect on the toxic response. This has been the foundation of the "fiber paradigm" stating that fibers meeting specific requirements represent a health hazard (Donaldson et al., 2010). In the present study on pulmonary toxicity, we have included an elongated form of anatase TiO_2 NM, which however do not fulfill the requirements of the fiber paradigm.

The main objectives of the present study was to assess pulmonary toxicity in terms of influx of inflammatory cells into the lung, pulmonary acute phase response, genotoxicity, and lung histopathology in mice exposed to four anatase TiO_2 NMs with different physicochemical properties (a large and a small NM, and a cube and a tube shaped NM) by i.t. instillation. In addition, we assess systemic toxicity in terms of hepatic acute phase response and genotoxicity. We compare the data on anatase TiO_2 NMs with previously published data on five rutile TiO_2 NMs in order to discuss the importance of the crystal phase on pulmonary inflammation. In addition, we discuss the significance of BET surface area, crystal phase and shape as possible predictors of pulmonary toxicity (neutrophil influx, acute phase response) by using multiple regression analyses.

2. Materials and methods

2.1. Nanomaterials and characterization

Four anatase TiO_2 NMs with varying physicochemical properties were included in the present study. The TiO_2 NMs with declared sizes of 15 nm, and 100 nm were obtained from MK Nano, Canada (MKN-A015 and MKN-A100, denoted TiO_2 NM-1 and TiO_2 NM-2, respectively). The TiO_2 NMs with shapes like a tube and a cube (denoted TiO_2 tube and TiO_2 cube, respectively) were obtained from partners in the SmartNanoTox project (Jožef Stefan Institute, Ljubljana, Slovenia). The quartz (DQ12) was included as benchmark particle (kindly provided from Craig Poland, University of Edinburgh, United Kingdom). CB, Printex 90, was used as internal reference material (a gift from Degussa-Hüls, Germany). The synthesis of the TiO_2 tube has been published elsewhere (Garvas et al., 2015). The description of the TiO_2 cube and TiO_2 tube synthesis is provided in the Supplementary material.

Morphology of the four anatase TiO_2 NMs and DQ12 was investigated with TEM (Jeol 2100, 200 kV). The specimens were prepared by probe sonication of NMs (TiO_2 NM-1, TiO_2 NM-2 and TiO_2 tube) in the suspension used for i.t. instillation (method described below) while DQ12 and TiO_2 cube NMs were dispersed ultrasonically in MeOH for 20 min. Then one drop of dispersion was deposited on a lacey carbon film supported by a copper grid.

The phase composition of the samples was determined with X-ray powder diffraction (XRD), using a D4 Endeavor, Bruker AXS diffractometer with Cu Kα radiation (λ = 1.5406 Å) and a Sol-X energy-dispersive detector. Diffractograms were measured in the 2θ angular range between 5 and 80° with the step size of 0.02°/s and the collection time of 3 s.

Specific surface areas were determined by the Brunauer, Emmett and Teller method (referred to as the BET method) by Quantachrome Instruments (Boynton Beach, FL, USA). In brief, nitrogen adsorption at 77.4 K was used for the determination of the specific surface. At the statistic-volumetric method, a specific amount of measuring gas is dosed onto the temperatured sample, which is arranged in vacuum. The samples were prepared at 250 °C, under vacuum, for 2 h and analysis were performed on a QUANTACHROME Quadrasorb.

2.2. Acellular oxidation potential

The $DCFH_2$-DA assay is one of the most used assays to measure reactive oxygen species (ROS) formation (Møller et al., 2010). In cellular assays, cells are loaded with the compound $DCFH_2$-DA, which is hydrolyzed intracellularly by endogenous esterases, whereas chemical deacetylation in NaOH is required when performing acellular assays. Here we measure the acellular oxidation potential of NMs as previously described (Bengtson et al., 2016). In brief, particle suspensions in Hanks buffered saline solution (HBSS) were probe sonicated on ice, for 16 min with 10% amplitude without pause, using a Branson Sonifier S-450D (Branson Ultrasonics Corp., Danbury, CT, USA) equipped with a disruptor horn (model number 101–147-037). $DCFH_2$-DA was hydrolyzed to 2′,7′-dichlorodihydro fluorescein ($DCFH_2$) by NaOH and diluted in HBSS. The particle suspensions with concentrations ranging from 0 to 200 μg/ml and $DCFH_2$ (0.01 mM) was added to 96-well plates and incubated for 3 h. The level of DCF was measured at excitation and emission wavelengths of 490 and 520 nm, respectively (Victor Wallac-21,420, Perkin Elmer, Denmark).

2.3. Preparation of instillation suspensions and characterization

The TiO_2 NMs and DQ12 were suspended in Nanopure water added 2% *v*/v C57BL/6 mouse serum to a final concentration of 3.24 mg/ ml and probe sonicated on ice, for 16 min with 10% amplitude without pause, using a Branson Sonifier S-450D (Branson Ultrasonics Corp., Danbury, CT, USA) equipped with a disruptor horn (model number 101–147-037). The final concentration of 3.24 mg/ml corresponds to the highest dose of 162 μg per 50 μl, which were the instillation volume per mice. The instillation suspensions were further diluted three-fold times to obtain 54 and 18 μg per 50 μl, respectively and sonicated for 2 min. The vehicle of Nanopure water added 2% v/v C57BL/6 mouse serum was similarly sonicated as just described.

The average hydrodynamic particle size of the anatase TiO_2 NMs in instillation suspensions (3.24 mg/ml) were determined by Dynamic Light Scattering ((DLS); Malvern Nano Zetasizer equipment mounted with a 633 nm red laser) as described previously (Saber et al., 2016; Modrzynska et al., 2018a, 2018b). Data were obtained from six repeated analyses of the same sample.

Endotoxin levels were measured using the Kinetic-QCL™ Kinetic

Table 1
Main physiochemical parameters of the NMs.

Name	NM-type	Source	Size (range)[c]	Morphology[c]	BET (m^2/g)	Endotoxin EU/ml[d]
TiO_2 NM-1	Anatase TiO_2[a]	MK Nano	12–50 nm	rectangular/spherical	84.6	0.117
TiO_2 NM-2	Anatase TiO_2[a]	MK Nano	16–28 nm	rectangular/spherical	73.5	0.156
TiO_2 tube	Anatase TiO_2	this study	length: 40–500 nm diameter: 6–11 nm	tube	154	0.095
TiO_2 cube	Anatase TiO_2	this study	a = 11–17 nm b = 15–27 nm	cube/cube-like	96.9	0.112
DQ12	Quartz	IOM[b]	50-400 nm	different	10.1	0.094

[a] from XRD patterns an amount of rutile is present in TiO_2 NM-1 and TiO_2 NM-2 (11.5 wt% and 5.6 wt%, respectively).
[b] kindly provided by Dr. Craig Poland, Institute of Occupational Medicine, Edinburgh, Scotland.
[c] based on TEM analysis.
[d] the level of endotoxin in Nanopure water with 2% mouse serum was 0.112 EU/ml.

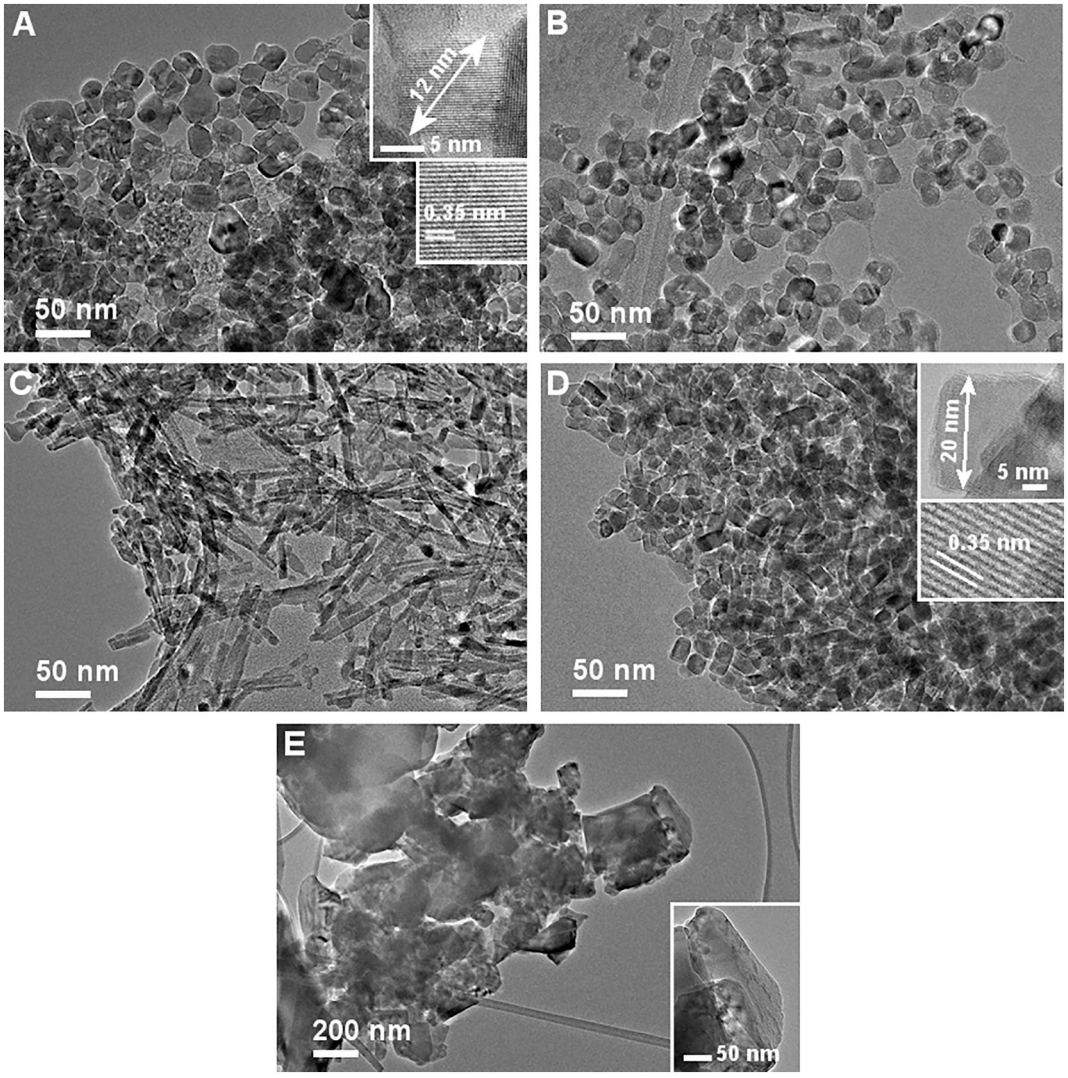

Fig. 1. TEM images of TiO_2 NM-1 (A), TiO_2 NM-2 (B), TiO_2 tube (C), TiO_2 cube (D) and DQ12 (E).

Chromogenic Limulus Amebocyte Lysate Assay Kit (Lonza, Walkersville, MD, USA) as described previously (Saber et al., 2012a).

The doses 18, 54 and 162 μg/mouse are equivalent to 1.5, 5 and 15 working days at the 8-h time-weighted average occupational exposure limit for TiO_2 by Danish Regulations (6.0 mg/m^3 TiO_2) (Jackson et al., 2013a).

2.4. Animal handling and exposure

Seven-week-old female C57BL/6jBomtac mice (Taconic, Ejby, Denmark) were randomized to either polypropylene cages containing animals for NM exposure (N = 7 mice/group for BAL and tissue collection and N = 5 mice/group for histology) or to cages containing vehicle controls (N = 2–4 mice/group). The animal experiments were performed over several weeks and vehicle controls were included on each exposure day. The vehicle controls were combined for each post-

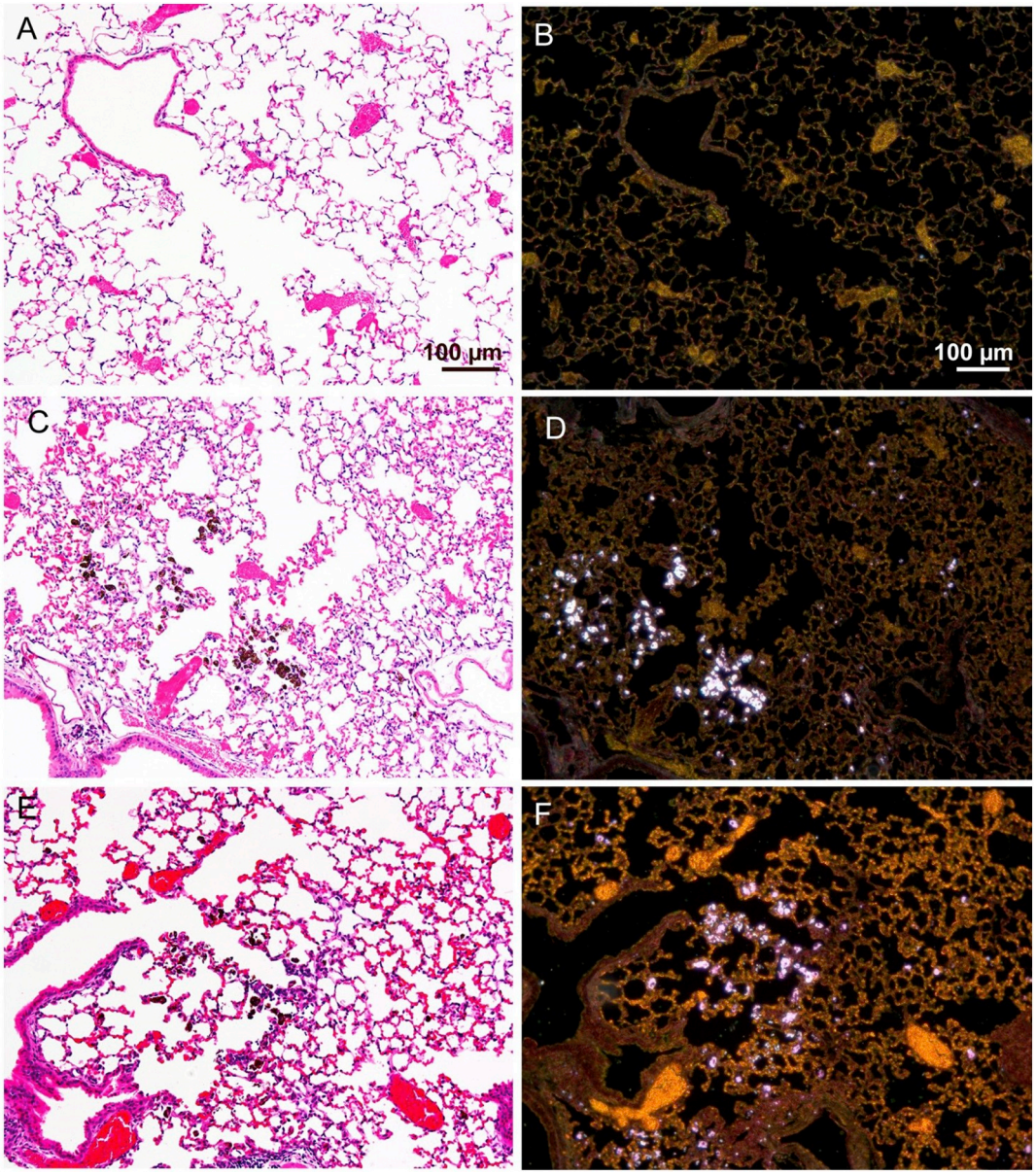

Fig. 2. Mouse lung histopathology and particle distribution 28 days post-exposure to (A, B) vehicle control, (C, D) TiO_2 NM-1 and (E, F) TiO_2 NM-2. (C, E, brightfield) Minor macrophage activity and (D, F, darkfield) focal distribution of nanomaterial (white) in the alveolar region. Brightfield and enhanced darkfield microscopy, H&E stain, scale bar 100 µm applies to all.

exposure day; $N = 15$ (day 1 and 3) and $N = 10$ (day 28, 90, 180) per dose group. The mice had access to food (Altromin 1324) and water ad libitum. The housing conditions have been described in detail elsewhere (Hadrup et al., 2017). At 8 weeks of age the mice were anesthetized and exposed to 50 µl anatase TiO_2 NMs, DQ12 or vehicle by single i.t. instillation. Mice for 180 days exposure only received the highest dose of 162 µg. For histology doses of 500 and 1000 µg/mouse DQ12 were included. The instillation procedure has been described in detail previously (Jackson et al., 2010; Saber et al., 2012a; Hadrup et al., 2017). In brief, the mice were placed on their backs on a 40^0 slope. A diode light was placed touching the larynx and the trachea was intubated using a catheter. The 50 µl NM suspension was instilled followed by 150 ml air. The catheter was removed and the mouse transferred to a vertical hanging position with the head up. This ensures that the administered material is maintained in the lung and breathing was observed to assure that airways were not blocked (Jackson et al., 2010).

Animal experiments were performed according to EC Directive 2010/63/UE in compliance with the handling guidelines established by the Danish government and permits from the Experimental Animal Inspectorate (no. 2015-15-0201-00465). Prior to the study, the experimental protocols were approved by the local Animal Ethics Council.

2.5. Preparation of BAL and tissue collection

One, 3, 28, 90 or 180 days post-exposure mice were anesthetized and necropsied. The BAL collection procedure has been described in detail previously (Saber et al., 2012a; Hadrup et al., 2017). In brief, mice were anesthetized and lungs were flushed twice with sterile 0.9% sodium chloride through the trachea to obtain BAL fluid. The BAL fluid was kept on ice until separation of fluid and cells by centrifugation at 400 x*g* for 10 min at 4 °C. Small pieces of lung and liver tissue were snap frozen in cryotubes in liquid nitrogen and stored at 80 °C until isolation of RNA for mRNA expression analysis and sample preparation for the comet assay.

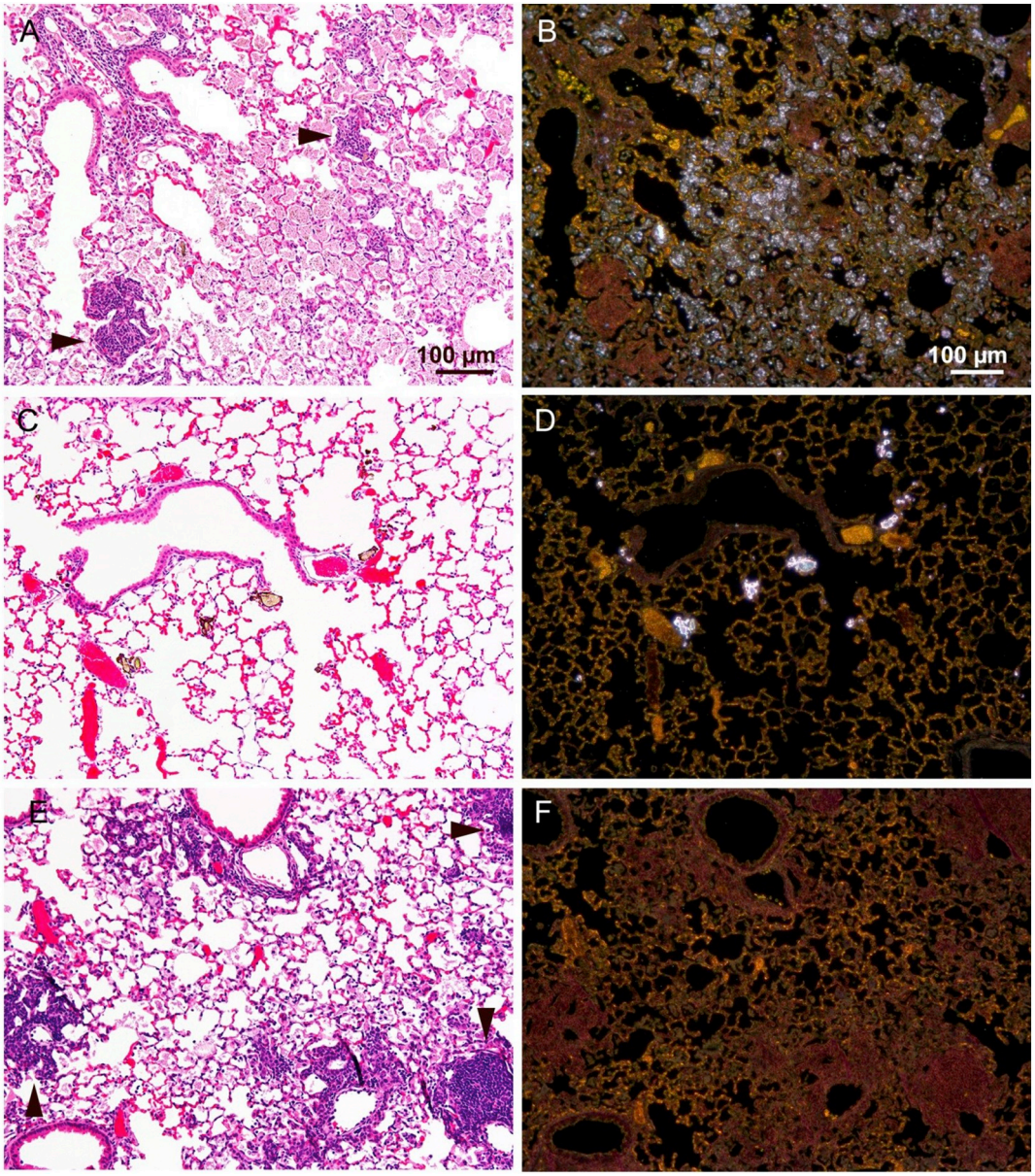

Fig. 3. Mouse lung histopathology and particle distribution 28 days post-exposure to (A, B) TiO_2 tube and (C, D) TiO_2 cube and 180 days post-exposure to (E) DQ12. (A and E) Lymphocytic infiltrates (arrow heads) and proteinosis in alveolar spaces in mice exposed to TiO_2 tube and DQ12. (B) Alveoli full of micron-sized agglomerates of TiO_2 tube (white). (D) TiO_2 cube (white) appeared mainly as scattered large aggregates. (F) DQ12 cannot be detected by darkfield microscopy. Brightfield and enhanced darkfield microscopy, H&E stain, scale bars 100 µm applies to all.

2.6. BAL cell differential counting

The separated BAL cells were re-suspended in 100 µl HAMF12 medium with 10% fetal bovine serum. 40 µl of the cell suspension was mixed with 160 µl medium containing 10% dimethyl sulfoxide (DMSO) and stored at −80 °C for later analysis in the comet assay. The total number of cells and of dead cells was determined from 20 µl diluted cell suspension by NucleoCounter NC-200 (Chemometec, Allerød, Denmark). 40 µl of the fresh cell suspension was collected on microscope slides by centrifugation at 60 xg for 4 min and then the cells were fixed with 96% ethanol and stained with May-Grünwald-Giemsa stain. Differential counts of macrophages, neutrophils, lymphocytes, eosinophils, and epithelial cells were determined by counting 200 cells/sample under light microscope (100× magnification).

2.7. mRNA expression of Saa

Pulmonary and hepatic acute phase response was assessed by the measurement of *Saa3* and *Saa1* mRNA expression levels, respectively, as described previously (Saber et al., 2009; Wallin et al., 2017). In brief, total RNA was isolated from frozen liver and lung tissue using Maxwell® 16 LEV simply RNA Tissue Kit (AS1280, Promega, USA) according to the manufacturer's protocol. Complementary DNA (cDNA) was prepared using TaqMan® reverse transcription reagents (Applied Biosystems, USA) as described by manufacturer's protocol. Total RNA and cDNA concentrations were measured on NanoDrop 2000c (ThermoFisher, USA). The *Saa3* and *Saa1* gene expression was determined by real-time reverse transcriptase polymerase chain reaction (RT-PCR) using TaqMan pre-developed reagents (Applied Biosystems, USA) and 18S as a reference gene. The samples were run in triplicates using ViiA7 Real-Time PCR detector (Applied Biosystems, USA). The relative expression was measured by the comparative C_T method. Negative

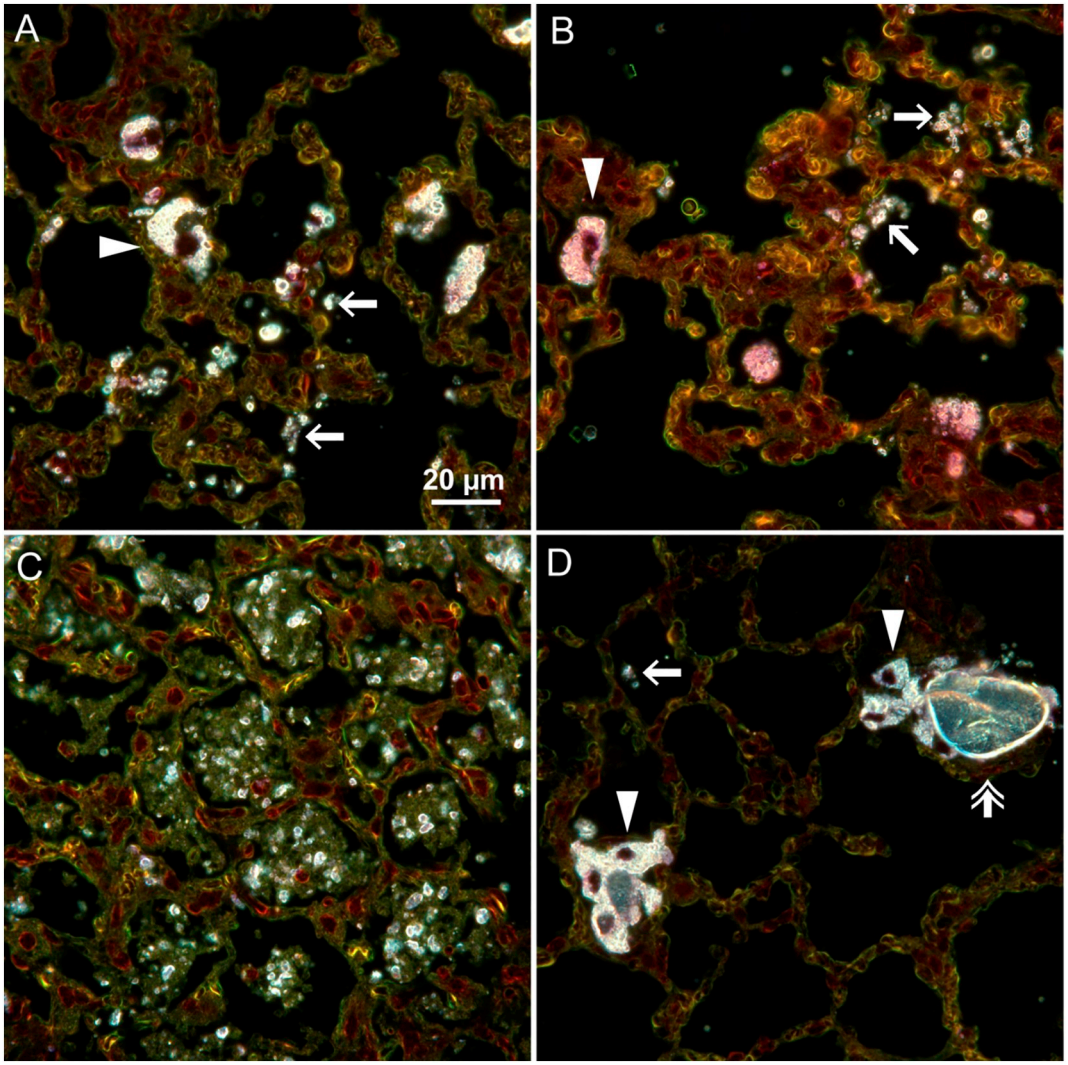

Fig. 4. Distribution and appearance of TiO_2 NM-1 (A), TiO_2 NM-2 (B), TiO_2 tube (C) and TiO_2 cube (D) in mouse lung 28 days post-exposure. All four TiO_2 NMs (white) appeared as micron-sized agglomerates in alveolar macrophages (arrow heads) or free in the alveolar lumen (arrows). (C) Alveoli full of micron-sized agglomerates of TiO_2 tube (white) and organic debris (green/grey). (D) TiO_2 cube appeared mainly as scattered large aggregates (double arrow). Enhanced darkfield microscopy, H&E stain, scale bar 20 µm applies to all. (For interpretation of the references to colour in this figure legend, the reader is referred to the web version of this article.)

controls were included in each run of the analysis. The day-to-day variation for the plate control in the analyses was 17.5% and 4% for *Saa3* and *Saa1*, respectively.

2.8. Comet assay

DNA strand breaks were determined by the comet assay on BAL cells, lung and liver tissue as described in (Jackson et al., 2013b; Modrzynska et al., 2018a, 2018b). In brief, single-cell suspensions were obtained by homogenization of frozen liver and lung pieces in ice-cold Merchant's buffer through a stainless steel mesh. The BAL cells were thawed in a 37 °C water bath before diluting with Merchant's buffer. The cell suspensions were embedded in agarose (0.7%) on microscope Trevigen 20-Well CometSlides™. The slides were immersed in cold lysing solution and stored overnight at 4 °C. Samples were treated with alkaline buffer and electrophoresis with circulating ice-cold electrophoresis buffer was performed (25 min, 38 V, 70-77A). Thereafter, slides were washed in neutralization buffer (0.4 M Tris, pH 7.5), fixed with 96% ethanol and stained with SYBRGreen®. DNA strand breaks were quantified as percentage of DNA in the comet tail (%TDNA) and as the comet tail length (TL). The comets were scored by the fully automated PathFinder™ system (IMSTAR, France). In order to control the day-to-day variation both negative (A549 human lung epithelial cell line treated with PBS for 30 min at 4 °C) and positive (A549 human lung epithelial cell line treated with 60 µM H_2O_2 for 30 min at 4 °C) controls were included. The samples were run over eight experiment days. The day-to-day variation for the negative and positive controls was 9% and 18% for TL, respectively.

2.9. Histopathology

At 28, 90 or 180 days post-exposure mice were weighed and anesthetized. Lungs were filled slowly with 4% formalin under 30 cm water column pressure. A knot was made around the trachea to secure formaldehyde in lungs to fixate tissue in “inflated state”. Lungs were then removed and placed in 4% neutral buffered formaldehyde solution for 24 h as previously described (Poulsen et al., 2016). After fixation the samples were trimmed, dehydrated on a Leica ASP300S (Leica Systems) and embedded in paraffin. Sections were cut at 3 µm on a Microm HM 355S Microtome (Thermo Scientific™). Sections for light microscopic examinations were stained with Haematoxylin and Eosin (H&*E*-staining) or Sirius Red staining. The sections were examined by light

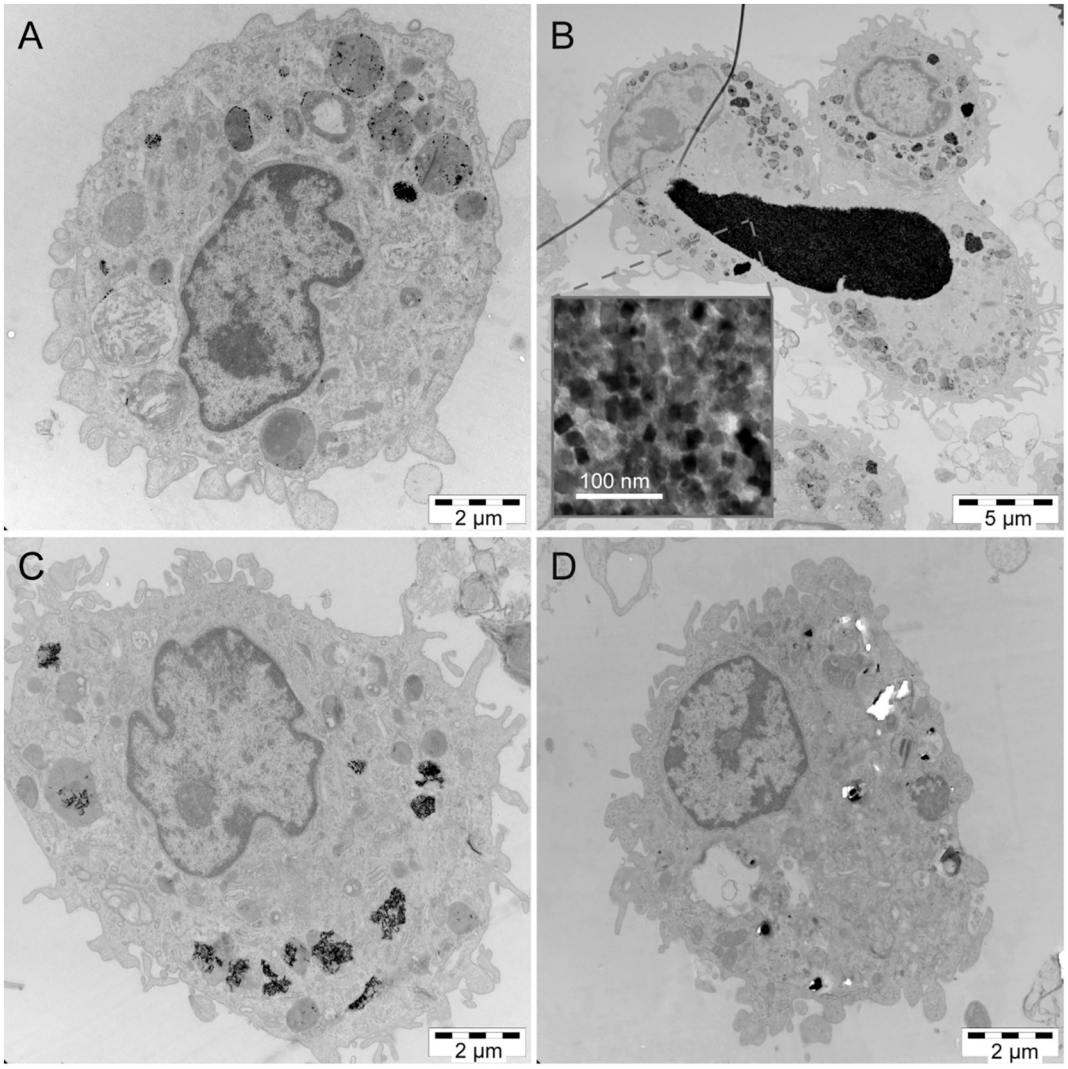

Fig. 5. Electron micrographs of subcellular distribution of (A, B) TiO_2 cube, (C) TiO_2 tube and (D) DQ12 in alveolar macrophages in bronchoalveolar lavage 90 days post-exposure. Insert in (B) is a high power image of the large aggregate of TiO_2 cubes.

microscopy using a Leica DM 4000B microscope equipped with a Leica DFC 480 camera and an Olympus BX43 microscope with a Nikon DS-Fi2 camera. Lymphocytic and macrophage infiltrates were defined as areas of tissue where the density of lymphocytes and macrophages were higher than the background. The minimum requirement was that they should contain 20 or more lymphocytes or 5 or more macrophages. The proteinaceous debris in the alveolar spaces was compatible with that seen in pulmonary alveolar proteinosis (PAP). The number refers to percentage of afflicted alveoli in the lobe. Granuloma formations refer to foreign body type granulomas with material surrounded by at least a few adherent macrophages and exclude giant cells.

2.10. Darkfield microscopy

Standard darkfield and Cytoviva enhanced darkfield hyperspectral system (Auburn, AL, USA) was used to detect particles in lung tissue by scanning histological sections at 10× and 40× magnification. Images were acquired at 10× on a Leitz Laborlux K microscope with a Leica MC170 HD camera and a 100× using an Olympus BX 43 microscope with a Qimaging Retiga4000R camera.

2.11. Electron microscopy

Samples were fixed in 2.5% glutaraldehyde and post fixed in 1% osmium tetroxide, dehydrated and embedded in LX-112. Thin sections were collected on carbon coated copper grids, stained with uranyl acetate and lead citrate. Grids were analyzed with a transmission electron microscope operated at 100 kV (JEM-1220, Jeol ltd, Japan, Tokyo) and photographed with Veleta TEM CCD camera (Olympus Soft Imaging Solutions GmbH, Germany). Preparation of TEM samples were done in Electron Microscopy Unit, University of Helsinki.

2.12. Statistical analysis

The data sets of BAL cells differential counting, mRNA expression, DNA strand breaks and histopathology were analyzed using the software package Graph Pad Prism 8.1.2. (Graph Pad Software Inc., La Jolla, CA, USA). All data are expressed as mean ± standard deviation. Data were tested for normality using the Shapiro-Wilks test and for variance homogeneity using the Bartlett's test. It was not possible to fulfill the normality and variance homogeneity criteria for most data by neither logarithmic nor cube root transformations. Therefore, the data were analyzed by the nonparametric Kruskal-Wallis test followed by Dunn's multiple comparison method as post hoc to test the differences between the test groups. *P*-value $\leq .05$ was considered significant.

To identify important TiO_2 NMs properties multiple regression analyses were conducted on the following endpoints: neutrophil influx in the BAL fluid and pulmonary *Saa3* expression. The four anatase and

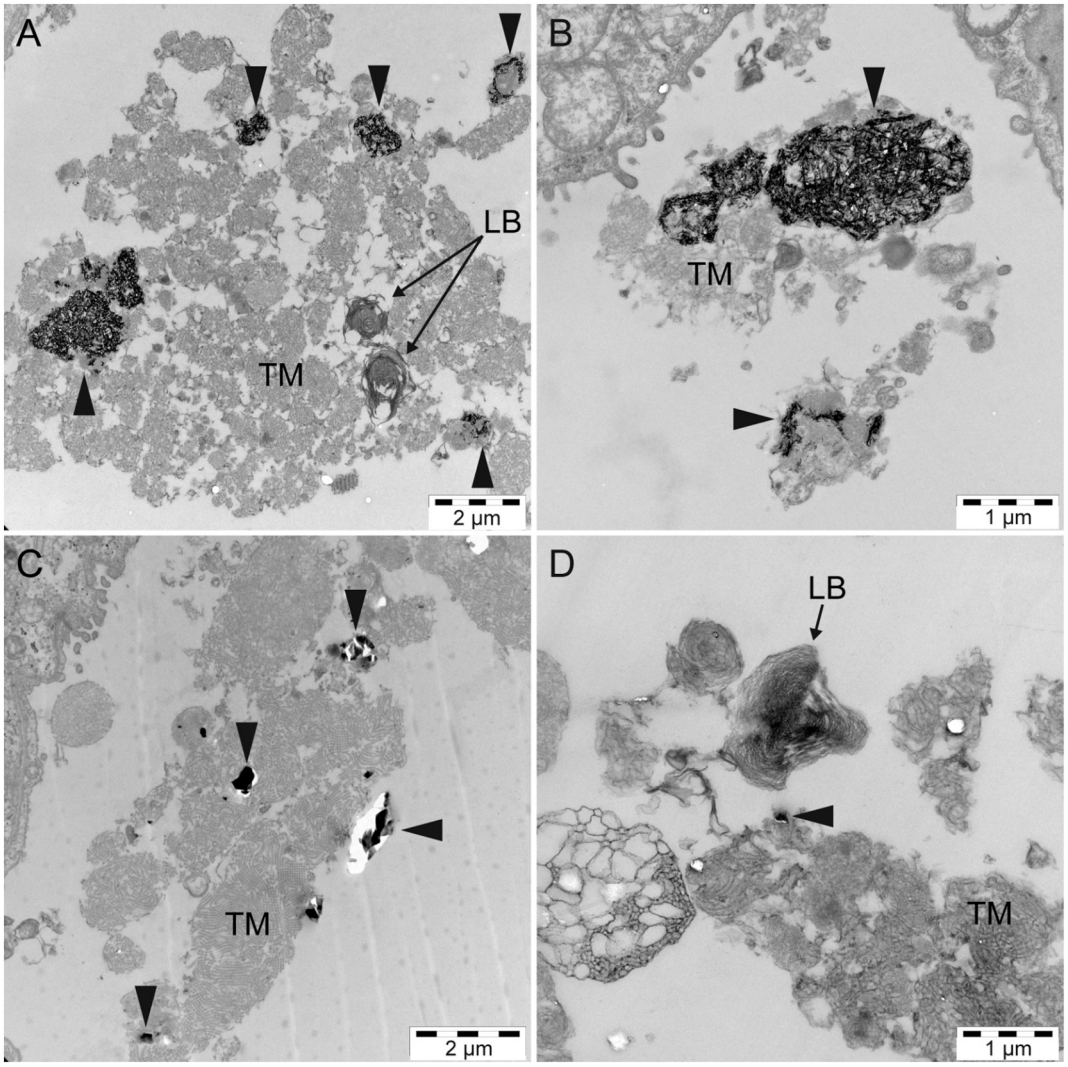

Fig. 6. Electron micrographs of alveolar proteinosis in mouse lung 90 days after exposure to (A, B) TiO_2 tube and (C, D) DQ12. Acellular organic debris (arrow heads), tubular myelin (TM) and lamellar bodies (LB).

the five rutile TiO_2 NMs were all included in the analyses. Selected physicochemical properties were: BET surface area, anatase phase, tube shape, and surface modification (NRCWE-002 and UV-Titan L181). Initially, a Pearson Correlation analysis was used to investigate the pairwise associations between physicochemical parameters (BET surface area, Anatase, Tube and Modified). No correlations between parameters were observed (results not shown), and all parameters were included as independent variables in the following multiple regression analyses. Multiple regression analyses investigating the relationship between physicochemical properties (BET surface area, Anatase, Tube and Modified) and neutrophil influx in the BAL fluid (all time points) or pulmonary *Saa3* expression (day 1 and 3 only), were performed. BET surface area was transformed using log(BET)/log(1.25), so the estimated effect corresponded to a 25% increase in BET. Statistical significance was determined at the 0.01 level in the multiple regression analyses, since no other correction for mass-significance was performed. The Pearson Correlations and all multiple regression analyses were performed in SAS version 9.4 (SAS Institute Inc., Cary, NC, USA).

3. Results

3.1. Physicochemical properties

The main characteristics of the anatase TiO_2 NMs and DQ12 are summarized in Table 1. Anatase TiO_2 NMs, labeled as TiO_2 NM-1, TiO_2 NM-2, TiO_2 tube, TiO_2 cube, and DQ12 were investigated with transmission electron microscopy (TEM) to determine particle morphology and size (Table 1). According to the supplier, TiO_2 NM-1 and TiO_2 NM-2 should have diameters of 15 and 100 nm, respectively. However, TEM of the anatase TiO_2 NMs (Fig. 1) revealed that the average diameter of the TiO_2 NM-1 particles (Fig. 1A) were around 30 nm and displayed a more rectangular than spherical shape. Only small amounts of the TiO_2 NM-1 particles had diameters around 10 nm. In addition, tiny particles with no certain shape and sizes below 10 nm were observed. The average diameter of the TiO_2 NM-2 particles (Fig. 1B) was 16 to 32 nm, instead of 100 nm which was the size reported by the manufacturer. These particles had a rectangular to spherical shape. The largest TiO_2 NM-2 particles were about 50 nm in diameter. However, these were not spherical, but rather elongated in one direction. The BET surface area of TiO_2 NM-1 and TiO_2 NM-2 was 85 and 74 m^2/g, respectively, indicating similar particle diameter sizes as confirmed by TEM. The TiO_2 tube NMs showed distinctive aggregates composed of tubes, while individual tubes was rarely observed (Fig. 1C). The outer diameter of the TiO_2 tube NMs varied from 6 to 11 nm and the length were up to 500 nm. The BET surface area was 154 m^2/g. The TiO_2 cube NMs had a rectangular shape (cube and cube-like (elongated in one direction)). The average size of the shorter side was about 17 nm and the longer side up to 26 nm. The particles were crystalline (Fig. 1D) and the BET surface

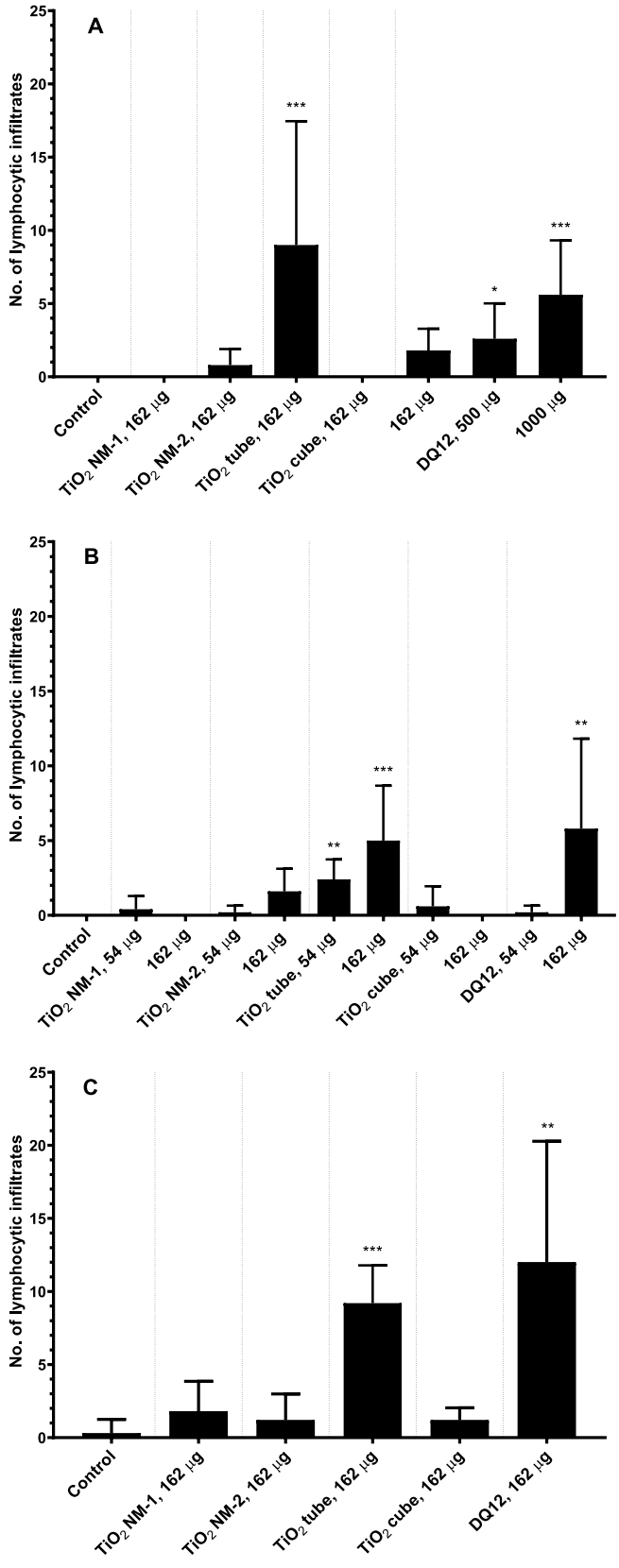

Fig. 7. Number of lymphocytic infiltrates based on histopathological evaluation of the lung tissue (A) 28 days, (B) 90 days (C) 180 days after a single i.t. instillation of TiO_2 NMs and DQ12.

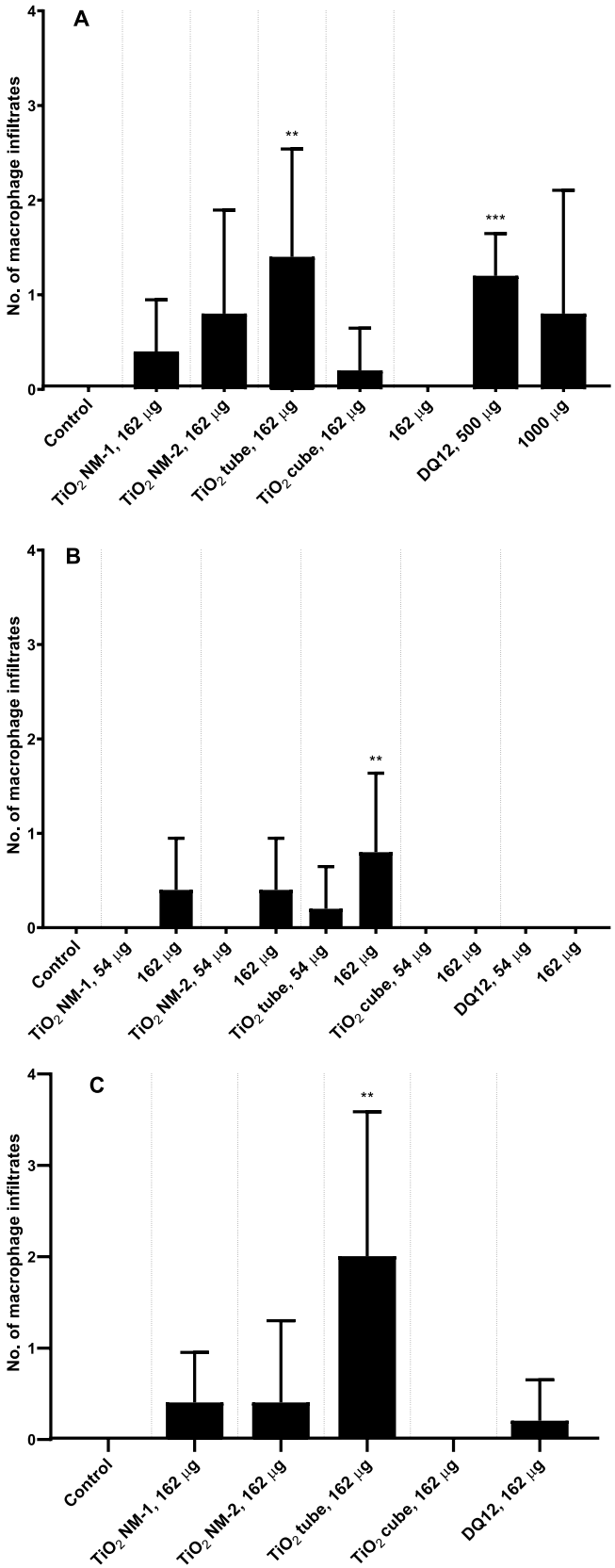

Fig. 8. Number of macrophage infiltrates based on histopathological evaluation of the lung tissue (A) 28 days, (B) 90 days (C) 180 days after a single i.t. instillation of TiO_2 NMs and DQ12.

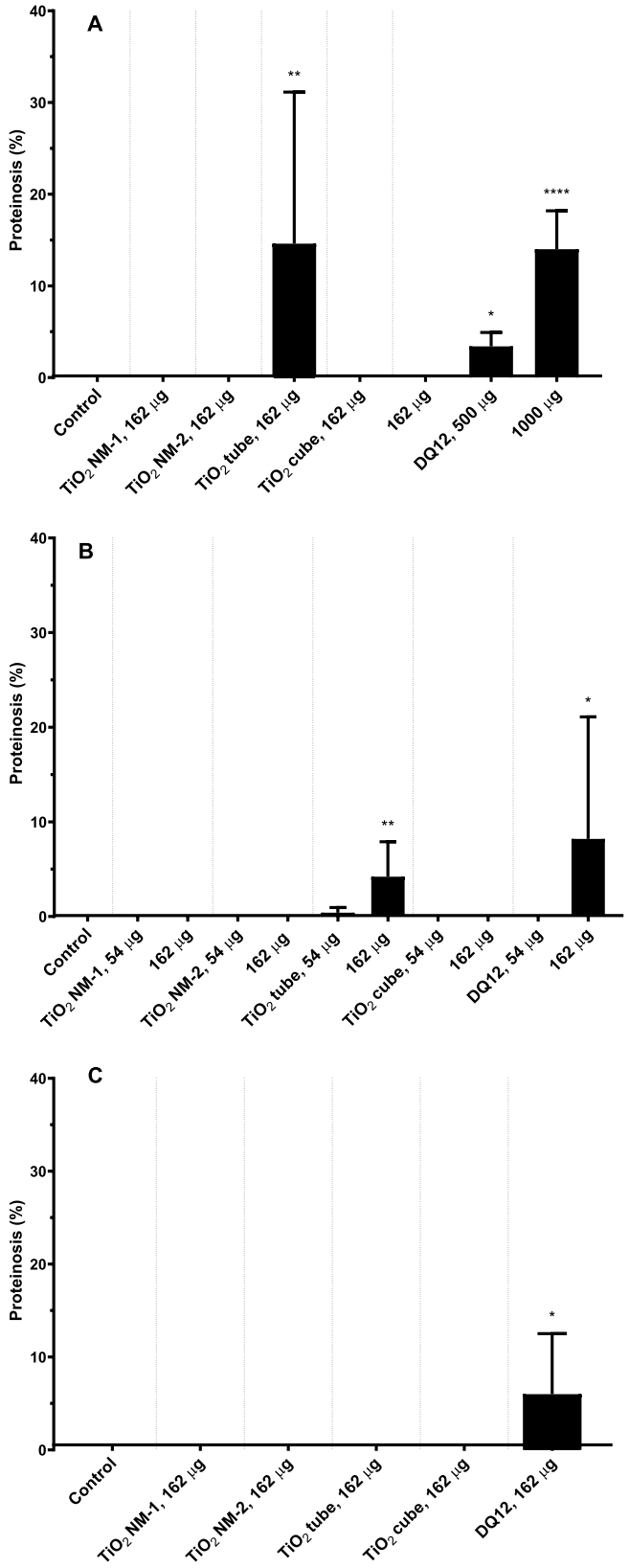

Fig. 9. Amount of protein debris (in percentage) based on histopathological evaluation of the alveolar spaces (A) 28 days, (B) 90 days (C) 180 days after a single i.t. instillation of TiO_2 NMs and DQ12.

area was 96.9 m^2/g. TEM of the DQ12 sample showed that the particles had different shapes and were unequally sized. The size ranged from 50 nm to 400 nm and aggregates, exceeding few micrometers, were observed. There was no presence of micropores as calculated by the t-Plot-method for any of the anatase TiO_2 NMs.

X-ray Diffraction (XRD) patterns of TiO_2 NMs (Supplementary material, Fig. S1) showed that TiO_2 NM-1 and TiO_2 NM-2 contained a small amount of rutile. The amount of rutile calculated using Spurr's formula was 11.5 wt% and 5.6 wt%, for NM-1 and NM-2 respectively. TiO_2 NM-2 also contained some unidentified impurities (arrows in Supplementary material, Fig. S1). For TiO_2 tube and TiO_2 cube all diffraction peaks corresponded to anatase structure (Supplementary material, Fig. S1).

Dynamic Light Scattering (DLS) was used to determine the hydrodynamic number-based size distributions of TiO_2 NMs and DQ12 in the instillation suspensions (3.24 mg/ml in Nanopure water with 2% mouse serum). The NM suspensions were generally well-dispersed and the size distribution showed unimodal peaks for TiO_2 NM-1, TiO_2 cube and DQ12 at 68 nm, 38 nm and 210 nm, respectively (Supplementary material, Fig. S2). TiO_2 NM-2 was bimodally distributed with a major peak at 50 nm and a minor broad peak at 18–38 nm. In addition, TiO_2 tube was bimodally distributed with a major peak at 60 nm and a narrow peak at 21 nm (Supplementary material, Fig. S2). The intensity-based z-average size and polydispersity index (PI) are shown in the Supplementary material, Table S1. The PI was between 0.4 and 0.7 indicating some polydispersity in the suspensions.

The endotoxin contents were measured using the *Limulus* Amebocyte lysate enzyme kit (LAL) and low levels were found in all NM suspensions (Table 1).

Characterization data on the five rutile TiO_2 NMs; NRCWE-001, NRCWE-002, NRCWE-025, NRCWE-030 and UV-Titan L181, were published previously (Saber et al., 2012b; Kermanizadeh et al., 2013; Gomez et al., 2014; Halappanavar et al., 2015) and summarized in the Supplementary material, Table S2.

3.2. Acellular oxidation potential

The ability to generate reactive oxygen species (ROS) was determined using the acellular 2′,7′-diclorodihydrofluorescein diactetate $DCFH_2$-DA assay as described previously (Jacobsen et al., 2008). All TiO_2 NMs and DQ12 generated ROS in a dose-dependent manner (Supplementary material, Fig. S3). There were no clear differences between rutile and anatase TiO_2 NMs, except that the rutile TiO_2 NM (NRCWE-002) induced a 7-fold larger ROS level than the others did.

3.3. Visualization of TiO_2 particles in the lung tissue

To assess the distribution and persistence of the NMs in the lung, histological sections of lung tissues were imaged using enhanced darkfield microscopy (Figs. 2, 3 and 4). TiO_2 NMs show intense light scattering in enhanced darkfield and are easily detected in tissues. DQ12 does not give an optical fingerprint in neither darkfield nor brightfield and therefore cannot be detected by optical microscopy (Fig. 3F). Darkfield microscopy of lung tissues 28 days post-exposure showed foreign material in the alveolar region for the four TiO_2 NMs (Figs. 2 and 3). TiO_2 NM-1 and NM-2 had a similar focal distribution (Figs. 2D, F) and a similar appearance as micron-sized agglomerates phagocytized by macrophages or scattered in the alveolar lumen (Figs. 4A, B). For the TiO_2 tube, there were areas of the lung tissue with alveoli full of micron-sized agglomerates and acellular organic debris (Figs. 3B and 4C), whereas the TiO_2 cube primarily appeared as scattered large aggregates (Figs. 3D and 4D). The TiO_2 tube and cube were also detected as micron-sized agglomerates in macrophages (only shown for TiO_2 cube in Fig. 4D). All four TiO_2 NMs were detected in lung tissue up to 180 days post-exposure (not shown).

Table 2
BAL fluid cell counts in mice 1, 3, 28 and 90 days post-exposure to 18, 54 and 162 μg TiO2 NMs, 162 μg DQ12 and control mice.

	Control		TiO_2 NM-1		TiO_2 NM-2		
	0 μg	18 μg	54 μg	162 μg	18 μg	54 μg	162 μg
1 day							
Neutrophils (× 10^3)	8.01 ± 5.95	6.57 ± 5.25	15.7 ± 10.5	49.6 ± 18.0**	9.15 ± 12.7	14.6 ± 9.66	50.2 ± 34.3**
Macrophages (× 10^3)	53.5 ± 17.7	51.4 ± 18.8	68.2 ± 17.1	44.6 ± 8.66	45.6 ± 29.7	57.3 ± 17.6	49.3 ± 16.3
Eosinophils (× 10^3)	0.96 ± 2.21	0.54 ± 0.80	0.56 ± 0.83	7.39 ± 7.55*	0.45 ± 1.05	0.29 ± 0.47	1.96 ± 1.70
Lymphocytes (× 10^3)	0.75 ± 0.56	0.64 ± 0.72	1.22 ± 1.49	1.88 ± 1.96	0.37 ± 0.18	1.11 ± 0.77	1.17 ± 0.49
Epithelial (× 10^3)	8.18 ± 4.23	10.9 ± 15.3	7.92 ± 3.64	5.38 ± 2.08	7.05 ± 7.08	9.49 ± 3.37	8.54 ± 4.86
Total BAL cells (× 10^3)	71.4 ± 20.1	70.2 ± 34.6	93.6 ± 23.3	109 ± 31.2	60.1 ± 40.9	82.8 ± 22.1	111 ± 25.1
3 days							
Neutrophils (× 10^3)	0.94 ± 1.25	0.64 ± 0.50	1.08 ± 0.87	11.4 ± 5.75**	0.69 ± 0.52	2.09 ± 1.87	5.53 ± 2.45*
Macrophages (× 10^3)	52.9 ± 8.72	56.4 ± 20.3	62.8 ± 17.1	62.4 ± 16.1	57.9 ± 10.9	64.5 ± 12.5	67.4 ± 28.9
Eosinophils (× 10^3)	0.05 ± 0.18	0.53 ± 0.42	3.89 ± 4.47	13.7 ± 13.3¤	0.70 ± 1.20	0.62 ± 0.66	9.89 ± 7.16¤
Lymphocytes (× 10^3)	0.90 ± 0.65	0.59 ± 0.70	1.93 ± 1.36	7.93 ± 8.64*	0.52 ± 0.38	1.06 ± 0.82	3.16 ± 2.20
Epithelial (× 10^3)	8.93 ± 9.08	8.72 ± 5.89	5.17 ± 3.28	5.49 ± 1.92	8.59 ± 3.80	13.9 ± 18.1	9.31 ± 9.50
Total BAL cells (× 10^3)	63.9 ± 13.1	66.9 ± 24.7	74.9 ± 19.1	101 ± 29.8	68.4 ± 13.6	82.1 ± 27.2	95.3 ± 41.4
28 days							
Neutrophils (× 10^3)	1.83 ± 2.41	1.74 ± 1.15	0.98 ± 0.67	2.82 ± 1.77	0.48 ± 0.59	1.28 ± 1.03	1.14 ± 0.75
Macrophages (× 10^3)	49.5 ± 10.6	60.6 ± 25.5	62.0 ± 8.51	52.9 ± 12.2	55.0 ± 14.9	45.6 ± 22.2	46.2 ± 18.6
Eosinophils (× 10^3)	0.47 ± 1.00	3.19 ± 4.29	0.59 ± 1.55	0.25 ± 0.51	0.17 ± 0.35	1.13 ± 2.56	0.08 ± 0.21
Lymphocytes (× 10^3)	1.88 ± 2.47	4.28 ± 3.13	2.91 ± 2.75	5.32 ± 3.56	0.90 ± 0.49	0.98 ± 0.75	2.46 ± 2.56
Epithelial (× 10^3)	7.85 ± 6.56	14.8 ± 10.9	6.74 ± 4.31	5.10 ± 4.08	6.43 ± 3.31	10.5 ± 14.9	6.99 ± 3.20
Total BAL cells (× 10^3)	61.5 ± 17.1	84.7 ± 26.5	73.2 ± 7.57	66.4 ± 13.3	63.0 ± 18.0	59.4 ± 26.7	56.9 ± 21.9

	TiO_2 tube			TiO_2 cube			DQ12
	18 μg	54 μg	162 μg	18 μg	54 μg	162 μg	162 μg
1 day							
Neutrophils (×10^3)	17.9 ± 6.05	115 ± 38.1#	186 ± 74.3¤	7.45 ± 4.17	4.66 ± 5.14	22.5 ± 15.1	116 ± 69.2#
Macrophages (×10^3)	55.6 ± 6.93	31.7 ± 10.2	22.8 ± 13.1*	54.1 ± 9.40	50.4 ± 22.2	55.9 ± 27.9	39.4 ± 10.3
Eosinophils (×10^3)	1.92 ± 3.70	6.08 ± 5.24*	10.3 ± 7.93**	0.04 ± 0.11	1.76 ± 3.22	2.00 ± 2.30	19.2 ± 30.2*
Lymphocytes (×10^3)	0.83 ± 0.73	1.85 ± 1.70	2.05 ± 1.26	0.98 ± 0.48	1.22 ± 1.21	1.52 ± 1.20	2.55 ± 3.10
Epithelial (×10^3)	7.89 ± 2.30	5.53 ± 2.72	4.56 ± 2.61	5.62 ± 2.38	8.95 ± 14.6	7.90 ± 3.23	5.84 ± 3.81
Total BAL cells (×10^3)	84.2 ± 15.6	160 ± 38.1**	226 ± 93.6¤	68.2 ± 8.29	67.0 ± 39.7	89.8 ± 31.5	183 ± 97.2**
3 days							
Neutrophils (× 10^3)	1.40 ± 1.06	26.9 ± 13.8¤	120 ± 28.7#	0.46 ± 0.40	0.26 ± 0.39	1.98 ± 1.41	18.2 ± 7.25**
Macrophages (×10^3)	79.9 ± 12.8*	69.7 ± 31.3	81.1 ± 21.3*	57.0 ± 14.0	70.6 ± 14.3	86.4 ± 26.2*	79.1 ± 27.4
Eosinophils (×10^3)	6.97 ± 9.00*	52.8 ± 22.9#	43.7 ± 28.7#	0.18 ± 0.27	0.17 ± 0.22	3.34 ± 4.06	28.0 ± 12.8#
Lymphocytes (×10^3)	1.73 ± 1.76	9.70 ± 8.00**	13.5 ± 4.12¤	0.84 ± 0.42	1.60 ± 0.87	1.47 ± 1.46	9.68 ± 8.83**
Epithelial (×10^3)	5.75 ± 2.20	10.7 ± 9.14	8.24 ± 4.03	4.51 ± 2.25	5.50 ± 3.24	7.89 ± 4.19	9.17 ± 9.13
Total BAL cells (×10^3)	91.2 ± 22.7	170 ± 59.4¤	267 ± 32.0#	63.0 ± 15.2	78.1 ± 15.2	101 ± 31.4	144 ± 41.9¤
28 days							
Neutrophils (×10^3)	5.66 ± 5.13	8.38 ± 3.83*	37.1 ± 16.5¤	0.56 ± 0.51	0.97 ± 1.31	0.41 ± 0.27	4.06 ± 3.07
Macrophages (×10^3)	63.9 ± 14.8	75.0 ± 18.9	133 ± 48.7**	50.9 ± 16.4	47.8 ± 17.4	59.8 ± 12.4	50.4 ± 22.9
Eosinophils (×10^3)	2.52 ± 2.65	0.46 ± 0.98	1.76 ± 2.86	1.51 ± 2.46	4.19 ± 9.13	0.93 ± 2.45	0.18 ± 0.34
Lymphocytes (×10^3)	5.04 ± 3.82	18.3 ± 13.9	55.5 ± 27.5	3.81 ± 5.39	2.46 ± 3.87	0.95 ± 0.73	13.9 ± 14.9
Epithelial (×10^3)	7.24 ± 6.90	8.40 ± 4.14	13.0 ± 8.02	4.07 ± 1.72	5.04 ± 2.70	5.62 ± 3.62	4.09 ± 2.85
Total BAL cells (×10^3)	82.8 ± 8.05	111 ± 25.0*	240 ± 88.8¤	60.8 ± 23.3	61.4 ± 17.0	67.7 ± 15.6	72.7 ± 35.5

All values are presented as mean ± SD. A symbol (*) denotes P ≤ .05, (**) P ≤ .01, (¤) P ≤ .001, (#) P ≤ .0001 compared to vehicle control.

3.4. Electron microscopy

TEM revealed that the NMs in the lungs were almost exclusively present in macrophages and mostly seen in phagosomal vesicles (Figs. 5A, C, D). As also noted in bright- and darkfield microscopy the TiO_2 cube formed large aggregates (Fig. 5B). The material in the aggregates appeared to be unchanged (Fig. 5B, insert).

The acellular organic debris associated with TiO_2 tube and DQ12 exposure visualized in darkfield microscopy was quite similar when using TEM (Fig. 6). Structures consistent with tubular myelin and lamellar bodies were identified. The findings in Fig. 6 conform to that seen in association with pulmonary alveolar proteinosis after quartz exposure (Corrin and King, 1970; Seymour and Presneill, 2002).

3.5. Histopathological analysis

The TiO_2 tube caused statistically significant increased inflammatory changes in lung tissue as defined by numbers of lymphocytic and macrophage infiltrates in the same manner as DQ12 compared to the control (Figs. 7 and 8). The other anatase TiO_2 NMs caused moderate inflammatory changes in the lung tissue. Macrophage infiltrations were not observed for DQ12 at 162 μg, in contrast to increased levels for TiO_2 tube at the same dose (Fig. 8). In addition to this a proteinaceous material was observed in the alveolar spaces of TiO_2 tube-exposed mice at day 28 post-exposure which was still present but at lower levels at day 90 post-exposure (Fig. 9). The same type of proteinaceous material was observed after exposure to DQ12, however the time course was different than for TiO_2 tube. For DQ12, at the 162 μg dose, the changes appeared later and persisted longer (Fig. 9). Increasing the dose of DQ12 to 500 μg or 1000 μg resulted in more

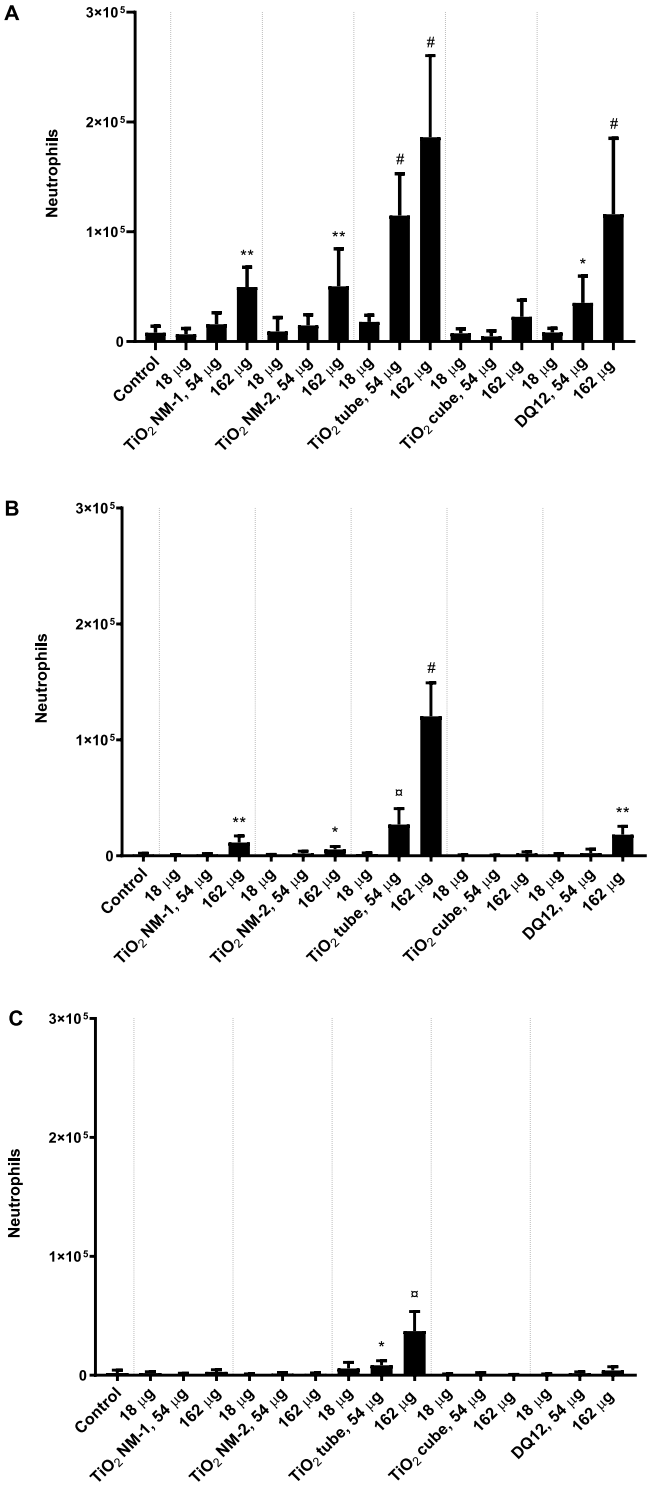

Fig. 10. Number of neutrophils detected in BAL fluid following a single i.t. instillation of 18, 54 or 162 µg of TiO_2 NMs and DQ12 measured (A) 1 day, (B) 3 days, and (C) 28 days post-exposure. All values are presented as mean ± SD. A symbol (*) denotes $P \leq .05$, (**) $P \leq .01$, (¤) $P \leq .001$, (#) $P \leq .0001$ of neutrophil levels in exposed groups versus vehicle control.

changes at day 28 post-exposure (Fig. 9A). Proteinaceous material in the alveolar spaces in quartz-exposed animals and humans are a well-known effect and are termed pulmonary alveolar proteinosis (PAP) (Corrin and King, 1970; Seymour and Presneill, 2002). No granulomas were observed in the present study (data not shown). No signs of fibrosis were observed (data not shown).

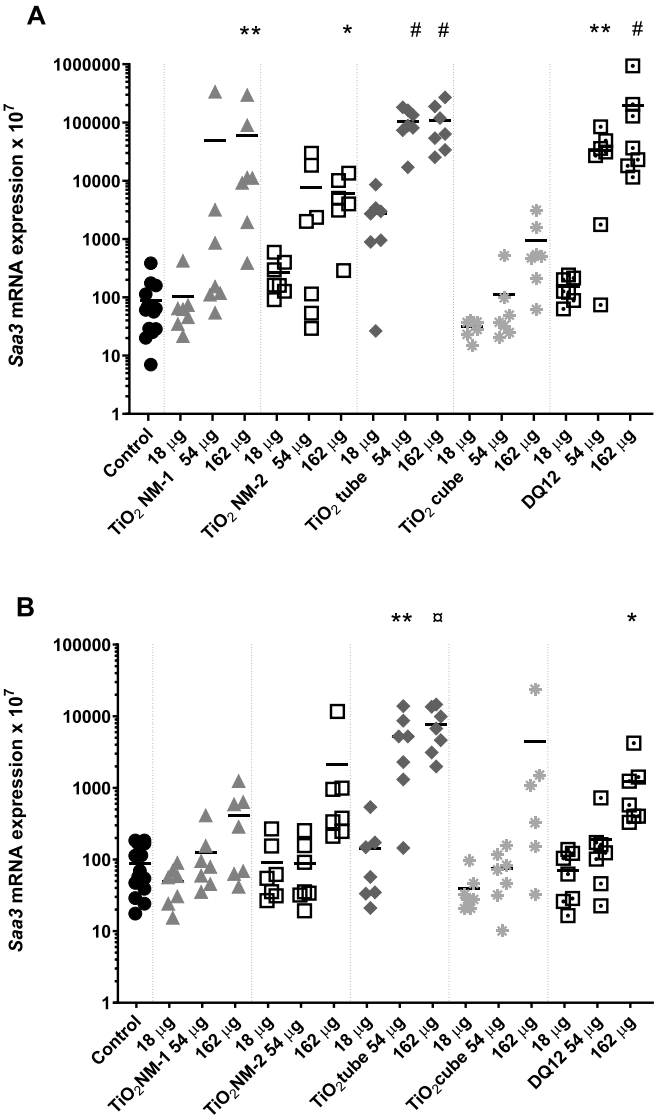

Fig. 11. Pulmonary mRNA expression levels of *Saa3* (A) 1 day and (B) 3 days after a single i.t. instillation of 18, 54 or 162 µg TiO_2 NMs and DQ12. All values are presented as mean ± SD at a logarithmic scale. A marker (*) denotes $P \leq .05$, (**) $P \leq .01$, (¤) $P \leq .001$, (#) $P \leq .0001$ compared to vehicle control.

3.6. Cell composition in bronchoalveolar lavage fluid

Recruitment of inflammatory cells in BAL fluid was assessed 1, 3, 28, 90 and 180 days post-exposure as a marker of the pulmonary inflammatory response. The distributions of total number of cells and the number of macrophages, neutrophils, eosinophils, epithelial and lymphocytes were determined (Table 2 (1, 3 and 28 days post-exposure) and Supplementary material, Table S3 (90 and 180 days post-exposure).

Dose-dependent neutrophil influx was observed at day 1 and 3 post-exposure for DQ12 and all the anatase TiO_2 NMs with exception of TiO_2 cube (Fig. 10). The number of neutrophils decreased over time after exposure. For the TiO_2 tube, the number of neutrophils, macrophages, lymphocytes and total BAL cells was statistically significant increased at day 28 post-exposure, which were the only observed inflammatory responses at that time-point. No statistically significant inflammatory responses were observed at the lowest dose of 18 µg or at 90 days post-exposure, except for a borderline statistically significant increase in the number of lymphocytes for TiO_2 tube 90 days post-exposure (162 µg, *P*-

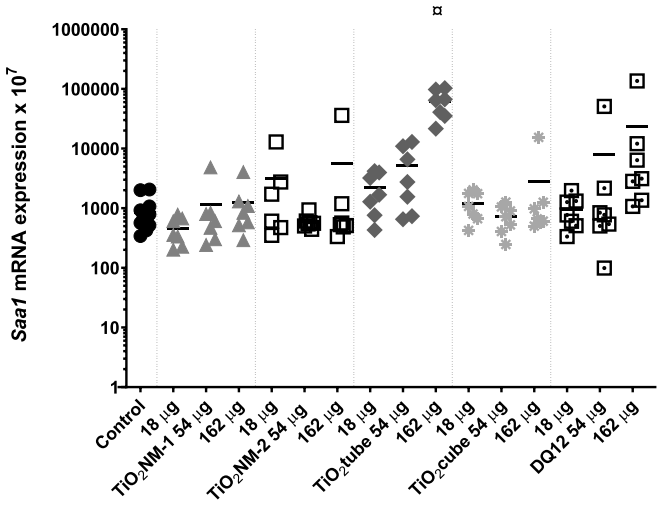

Fig. 12. Hepatic mRNA expression levels of *Saa1* 1 day after a single i.t. instillation of 18, 54 or 162 µg TiO_2 NMs and DQ12. All values are presented as mean ± SD at a logarithmic scale. A marker (*) denotes P ≤ .05, (**) P ≤ .01, (¤) P ≤ .001, (#) P ≤ .0001 compared to vehicle control.

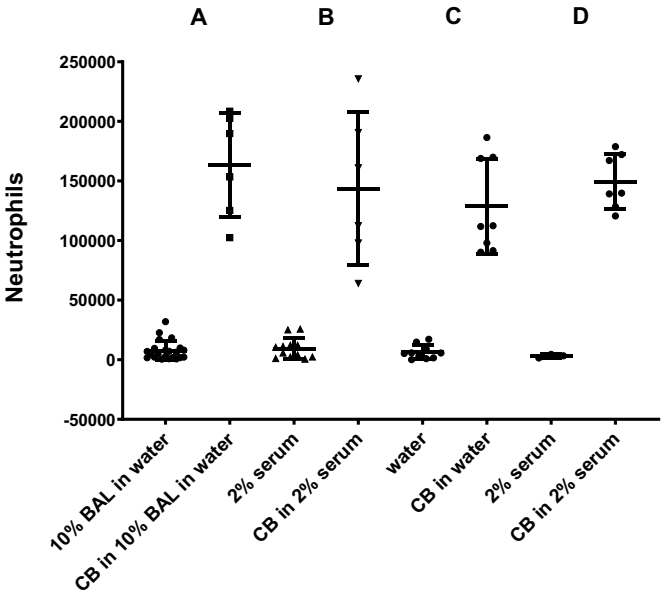

Fig. 13. Carbon black (Printex 90) was included (162 µg/mouse) in the previous studies on rutile TiO_2 NMs. A: (Saber et al., 2012a, 2012b (UV-Titan L181); B: Saber et al. 2018 (NRCWE-025 and -030); C: Wallin et al., 2017 (NRCWE-001 and -002) and D: this study on anatase TiO_2 NMs.

value: 0.068). However, statistically significant increased levels of neutrophils (7-fold) and lymphocytes (6-fold) was seen for TiO_2 tube 180 day post exposure to 162 µg. Overall, the TiO_2 tube generated a higher inflammatory response than the other TiO_2 NMs, whereas TiO_2 cube did not generate an inflammatory response.

3.7. Acute phase response

Pulmonary and hepatic acute phase response was assessed using *Saa3* and *Saa1* mRNA expression levels as biomarkers of pulmonary and hepatic acute phase response, respectively (Poulsen et al., 2017). The *Saa3* gene expression was statistically significantly increased 1-day post-exposure compared to vehicle control at the highest dose (162 µg) for DQ12 and all anatase TiO_2 NMs except for TiO_2 cube (Fig. 11). The TiO_2 tube and DQ12 also induced statistically significantly increased *Saa3* mRNA levels at the middle dose (54 µg) 1-day post-exposure. The significant increase of *Saa3* mRNA expression was persistent at day 3 post-exposure for TiO_2 tube (54 and 162 µg) and for DQ12 (162 µg), though the level was 10 times lower than observed at day 1. A strong correlation was observed for *Saa3* mRNA expression and neutrophil influx day 1 post-exposure (Supplementary material, Fig. S4).

One day post-exposure hepatic *Saa1* mRNA expression was statistically significant increased only for TiO_2 tube at the highest exposure dose (70-fold) (Fig. 12). *Saa1* expression levels at post-exposure day 3 were not analyzed.

3.8. Comet assay

DNA strand break levels were assessed in BAL cells, lung and liver tissue by the comet assay (Supplementary material, Table S4). There were only few significant increases in DNA strand break levels. However, DNA strand break levels were also observed to be statistically significantly decreased for some of the TiO_2 NMs, especially in the lung tissue, at different time points. The observed changes were in general not dose-dependent and considered as chance findings.

3.9. Correlations between neutrophils and BET surface area

The toxicological response to anatase TiO_2 NMs was compared to previously published studies on rutile TiO_2 NMs (Supplementary material, Table S2, (Jacobsen et al., 2009; Bourdon et al., 2012; Saber et al., 2012b). Carbon black (CB), (Printex 90), was included as reference material to allow comparisons across studies. CB (162 µg/mouse) used in the previous studies on rutile TiO_2 NMs resulted in similar levels of neutrophil influx as observed in the present study on anatase TiO_2 NMs (Fig. 13).

This comparison of anatase and rutile TiO_2 NMs was performed for acute inflammation as measured by neutrophil influx into the lung (BAL fluid) adhering to the method described by Schmid and Stoeger, 2016 (Schmid and Stoeger, 2016). This approach calls for normalization of the neutrophil number to the total number of cells in the BAL (PMN in %) and normalization of the instilled NM surface area dose to the average weight of mouse lungs (0.18 g). We found strong logistic correlations between surface area dose and level of neutrophil influx 1-day post-exposure for anatase TiO_2 NMs *without* TiO_2 tube (R^2 = 0.95) and rutile TiO_2 NMs (R^2 = 0.99), Fig. 14A. Clearly, all anatase and all rutile TiO_2 NMs represent two distinct dose-response curves with rutile showing somewhat enhanced surface-specific inflammogenicity. Interestingly, the anatase TiO_2 tubes (R^2 = 0.99) show enhanced inflammogenicity matching the (spherical) rutile rather than the (spherical, cubic) anatase TiO_2 NMs toxicity. Again referring to the approach presented by Schmid and Stoeger (Schmid and Stoeger, 2016) this can be quantified by considering the equivalent doses inducing 30% PMN influx into the lung ($dose_{30\%PMN}$), which represents a severe inflammation. As seen from Fig. 14B, the inflammogenicity of anatase TiO_2 tubes ($dose_{30\%PMN}$ = 200 cm^2/g) agree within experimental uncertainties (95% confidence level, CL = ±1.5-fold $dose_{30\%PMN}$) with that of rutile (spherical) TiO_2 NMs (170 cm^2/g; 110–260 cm^2/g (95% CL)), while spherical (and cubic) anatase TiO_2 NMs show a 3.2-fold less inflammogenicity ($dose_{30\%PMN}$ = 550 (370–830) cm^2/g). Interestingly, also Printex 90 (P90) shows the same surface-specific inflammogenicity as rutile TiO_2 NMs ($dose_{30\%PMN}$ = 220 cm^2/g).

3.10. Multiple regression analyses

With the aim of identifying TiO_2 NMs properties important for their toxicity, the effect of dose, BET surface area, crystal phase and shape on neutrophil influx and *Saa3* expression after i.t. exposure to both anatase and rutile TiO_2 NMs was analyzed by multiple regression (Tables 3 and 4). Mass dose significantly predicted neutrophil influx on all post-exposure days. Increasing BET surface area significantly predicted

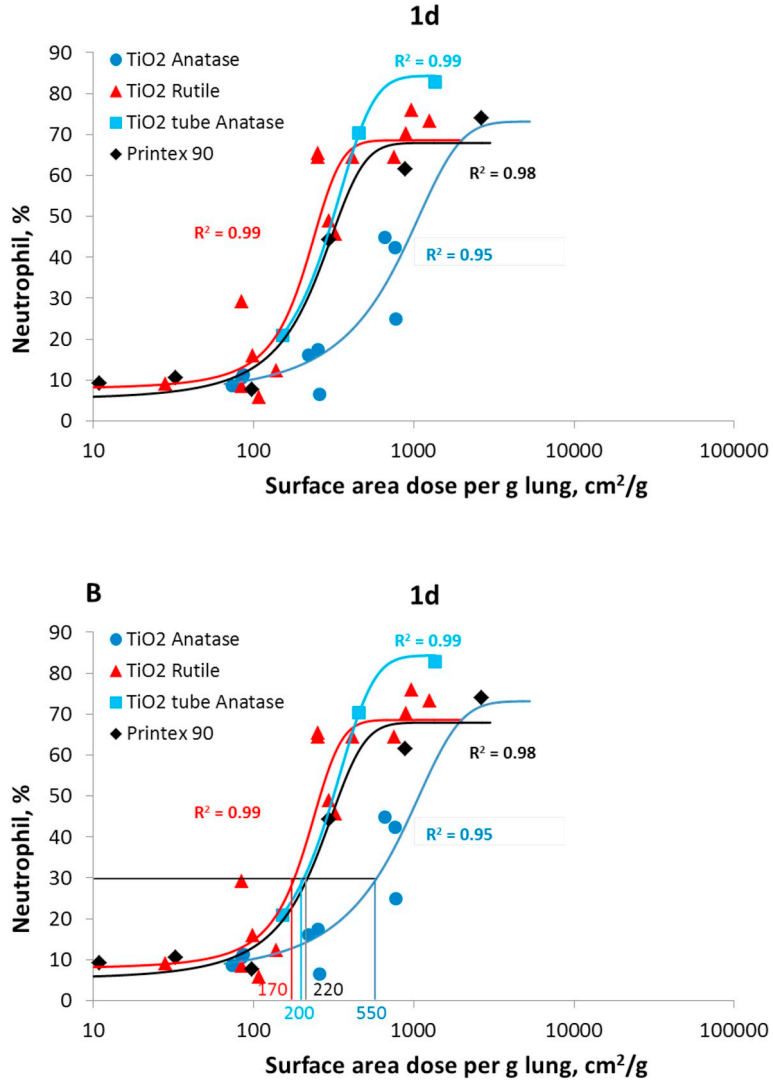

Fig. 14. Correlations between surface area dose and neutrophil influx for: A) rutile and anatase TiO_2 NMs; B) rutile and antase TiO_2 with TiO_2 tube shown seperately; C) TiO_2 tube and CNTs.

enhanced neutrophil influx 3 and 28 days post-exposure. The anatase phase predicted lower neutrophil influx 1 and 3 days after exposure. The tube shape significantly predicted increased neutrophil influx on all post-exposure days. When tube shape was included as a variable, the effect of BET surface area disappeared, suggesting that the crystal phase anatase/rutile and shape (tube) might be more important predictors than the BET surface area.

Mass dose and BET surface area (i.e. surface area dose) significantly predicted *Saa3* expression on all post-exposure days (1 and 3 days). The tube shape significantly predicted increased *Saa3* expression at both post-exposure days. When tube shape was included as a variable, again the effect of BET surface area disappeared. At 3 days post-exposure the anatase phase predicted lower neutrophil influx.

There was no effect of surface modifications (rutile NRCWE-002 and rutile UV-Titan L181), data not shown.

4. Discussion

Inhalation exposure is the gold standard for risk assessment. However, the i.t. instillation technique used in the present study is generally well-accepted for hazard ranking of different NMs (Warheit et al., 2005; Baisch et al., 2014). The i.t. instillation technique has shown an even distribution of NMs including MWCNT across most lung-tissue sections (Mikkelsen et al., 2011; Poulsen et al., 2016). However, compared to inhalation the i.t. instillation results in a more patchy distribution as shown using fluorescent nanoparticles (Yang et al., 2019). Recently, a study concludes that neutrophil influx from i.t.- and inhalation-exposed rats correlated with the estimated pulmonary deposited surface area across both types MWCNT and types of exposure at two different time points (Gate et al., 2019). Additionally, it has been shown that global pulmonary transcriptomic pattern following i.t. instillation and inhalation of TiO_2 NMs in mice is remarkably comparable (Halappanavar et al., 2011; Husain et al., 2013), suggesting common biological responses between administration methods. The doses used in the present study reflect occupationally relevant exposure levels and allow comparison with previously performed animal studies using the same dose levels (e.g. the rutile TiO_2).

The study was designed to cover a wide NM size range. Unexpectedly, the BETs for the two TiO_2 NMs with a small and large diameter size as reported by the manufacturer (TiO_2 NM-1 and TiO_2 NM-2) showed to be similar. This was confirmed by TEM. Thus, the optimal study design having a wide BET range with larger surface areas was compromised.

The greatest overall inflammatory response was seen for neutrophil influx 1 and 3 day post-exposure, especially for the TiO_2 tube and DQ12. In addition, the total number of cells, lymphocytes and

Table 3
Multiple regression analyses.

	Neutrophil influx				
	Exposure Variable	Multiplicative Effect	Lower CL	Upper CL	Probt
1 day	**Dose**	**1.016**	**1.011**	**1.020**	**<0.0001**
	Per 25% difference in BET	1.052	0.910	1.216	0.491
	Anatase	**0.307**	**0.173**	**0.544**	**<0.0001**
3 days	**Dose**	**1.030**	**1.023**	**1.038**	**<0.0001**
	Per 25% difference in BET	**1.370**	**1.094**	**1.716**	**0.0065**
	Anatase	**0.154**	**0.063**	**0.374**	**<0.0001**
28 days	**Dose**	**1.017**	**1.011**	**1.023**	**<0.0001**
	Per 25% difference in BET	**1.289**	**1.065**	**1.559**	**0.0094**
	Anatase	0.697	0.328	1.484	0.3477

	Neutrophil influx				
	Exposure Variable	Multiplicative Effect	Lower CL	Upper CL	Probt
1 day	**Dose**	**1.016**	**1.011**	**1.020**	**<0.0001**
	Per 25% difference in BET	0.912	0.785	1.060	0.230
	Anatase	**0.191**	**0.107**	**0.342**	**<0.0001**
	Tube	**10.23**	**3.783**	**27.65**	**<0.0001**
3 days	**Dose**	**1.030**	**1.023**	**1.037**	**<0.0001**
	Per 25% difference in BET	1.125	0.888	1.424	0.328
	Anatase	**0.082**	**0.033**	**0.202**	**<0.0001**
	Tube	**26.36**	**5.439**	**127.7**	**<0.0001**
28 days	**Dose**	**1.017**	**1.011**	**1.023**	**<0.0001**
	Per 25% difference in BET	1.083	0.888	1.321	0.431
	Anatase	0.389	0.180	0.839	0.016
	Tube	**18.36**	**4.815**	**70.01**	**<0.0001**

Physiochemical parameters and the influence on neutrophil influx after exposure to anatase and rutile TiO_2 NMs in multiple regression analyses.
BET surface area was transformed using log(BET)/log(1.25), so the estimated effect corresponded to a 25% increase.
Significant *p*-values ($P < .01$) are highlighted in bold.

Table 4
Multiple regression analyses.

	***Saa3* mRNA**				
	Exposure Variable	Multiplicative Effect	Lower CL	Upper CL	Probt
1 day	**Dose**	**1.028**	**1.023**	**1.033**	**<0.0001**
	Per 25% difference in BET	**1.506**	**1.289**	**1.758**	**<0.0001**
	Anatase	0.871	0.456	1.663	0.675
3 days	**Dose**	**1.017**	**1.013**	**1.020**	**<0.0001**
	Per 25% difference in BET	**1.163**	**1.045**	**1.294**	**<0.0001**
	Anatase	0.789	0.511	1.218	0.283

	***Saa3* mRNA**				
	Exposure Variable	Multiplicative Effect	Lower CL	Upper CL	Probt
1 day	**Dose**	**1.028**	**1.023**	**1.033**	**<0.0001**
	Per 25% difference in BET	1.217	1.047	1.413	0.0107
	Anatase	0.454	0.249	0.827	0.0102
	Tube	**29.73**	**11.16**	**79.16**	**<0.0001**
3 days	**Dose**	**1.017**	**1.013**	**1.020**	**<0.0001**
	Per 25% difference in BET	1.008	0.908	1.119	0.879
	Anatase	**0.500**	**0.331**	**0.754**	**0.001**
	Tube	**9.928**	**4.983**	**19.78**	**<0.0001**

Physiochemical parameters and the influence on *Saa3* mRNA levels after exposure to anatase and rutile TiO_2 NMs in multiple regression analyses.
BET surface area was transformed using log(BET)/log(1.25), so the estimated effect corresponded to a 25% increase.
Significant p-values ($P < .01$) are highlighted in bold.

eosinophils were significantly increased for the TiO_2 tube. In general, the other anatase TiO_2 NMs were somewhat less responsive, including the TiO_2 cube, which induced less inflammation than TiO_2 NM-1 and TiO_2 NM-2 despite its 20–30% larger specific surface area. The TiO_2 cube NMs had a peculiar tendency to form large aggregates in the lungs, which could be related to the relatively modest inflammatory response. DLS data for TiO_2 cube confirms a homogeneous instillation suspension without bigger aggregates, suggesting that this phenomenon happened in the lung. Persistent dose-dependent increases in the influx of inflammatory cells, including neutrophils, were observed up to 28 and 180 days post-exposure only for the TiO_2 tube suggesting that the difference in shape may be an important predictor for chronic lung inflammation.

We used *Saa3* mRNA levels in the lung as biomarker of the

pulmonary acute phase response and *Saa1* mRNA levels as biomarker for the hepatic acute phase response. Previous studies reported significant correlations between *Saa3* mRNA and protein levels in mice after MWCNTs exposure (Saber et al., 2014; Poulsen et al., 2015a; Poulsen et al., 2017). Consistent with the observed pulmonary inflammation the *Saa3* mRNA levels were dose-dependently increased 1 and 3 day post-exposure, again especially for the TiO_2 tube and DQ12. As in the present study, we have previously shown that pulmonary exposure to different NMs induce a pulmonary acute phase in parallel with the pulmonary inflammatory response (Bourdon et al., 2012; Saber et al., 2013; Poulsen et al., 2015a; Husain et al., 2013; Poulsen et al., 2017; Hadrup et al., 2019a; Hadrup et al., 2019b; Barfod et al., 2020).

The strong pulmonary inflammation of TiO_2 tube was accompanied by a hepatic acute phase response measured as increased *Saa1* mRNA levels at the highest dose 1-day post-exposure (70-fold increase). In previous studies, instillation of MWCNTs led to increased levels of both *Saa1* mRNA and SAA1 protein (Poulsen et al., 2017), whereas CB and rutile UV-Titan L181 TiO_2 did not (Saber et al., 2009; Halappanavar et al., 2011). The hepatic acute phase response may reflect the stronger surface area-dependent pulmonary inflammation induced by the TiO_2 tube, as pulmonary exposure to NRCWE-030 (spherical, rutile TiO_2) with a similarly large BET surface area (139 m^2/g) also induced hepatic *Saa1* mRNA levels (Modrzynska et al., 2018a, 2018b). The stronger response by the TiO_2 tube might be explained by a stronger adsorption of the TiO_2 tube onto cell membranes leading to the formation of membrane-wrapped nanoparticles allowing their relocation and diffusion into systemic circulation as recently shown (Urbancic et al., 2018).

DNA damage has been suggested to be caused by particle mediated ROS production and/or as a secondary consequence of an inflammatory response (Møller et al., 2010). The standard comet assay has been used in TiO_2 genotoxicity studies in cell cultures and animal models with mixed results, which might be due to physicochemical differences (Møller et al., 2017). The few changes (both increases and decreases) in DNA damage levels in BAL cells, lung and liver observed in the present study were considered as chance findings. Contrary, the rutile NMs have been able to induce DNA strand breaks in our previous animal studies (Saber et al., 2012b; Wallin et al., 2017). The acellular oxidation potential ($DCFH_2$-DA assay) of anatase and rutile TiO_2 NMs were in general similar, and cannot solely explain the difference in genotoxicity, although the rutile NRCWE-002 with the highest level of 2′,7′-dichlorofluorescein (DCF) also generated the highest level of DNA damage (Wallin et al., 2017).

Mice exposed to TiO_2 tube and the positive control DQ12 showed increased levels of macrophage and lymphocytic infiltrations as compared to the other NMs. None of the studied particles, including DQ12, induced fibrotic changes. However, both DQ12 and TiO_2 tube exposure resulted in accumulation of alveolar matter that was compatible with pulmonary alveolar proteinosis (PAP) (Corrin and King, 1970; Seymour and Presneill, 2002). Electron microscopy confirmed that the alveolar matter for both TiO_2 tube and DQ12 exposure was similar and that it conforms to the description of PAP in the literature (Crouch et al., 1991). In humans, PAP is a rare condition of mostly unknown etiology, but hereditary forms of this condition are known to exist (Seymour and Presneill, 2002). The secondary type of PAP is known to occur after exposure to crystalline quartz but it has also been associated with exposures to other mineral particles (talc, cement and kaolin) and metal particles (aluminum, titanium and indium) (Borie et al., 2011). Interestingly at the dose of 162 μg TiO_2 tube, there was a substantial amount of proteinosis 28 days post-exposure. However, this reaction subsided during time and had disappeared at 180 days post-exposure. In contrast, DQ12 at the same mass dose did not cause accumulation of alveolar matter until 90 days post-exposure and there was still substantial amounts 180 days post-exposure suggesting that the effect of DQ12 is more persistent than that of TiO_2 tube. The persistence of quartz-induced inflammation has been noted previously (Brown et al., 1991). However, it has to be noted that the BET surface area of TiO_2 tube is 15-fold larger than that of DQ12, i.e. for equivalent surface area dosing 2400 μg of DQ12 would have had to be dosed.

The length of the TiO_2 tube is not of the magnitude that it could be expected to cause asbestos-like effects as do some MWCNT. It is interesting that the effect of the TiO_2 tube shows similarities to DQ12 in terms of lymphocytic tissue inflammation and the ability to cause PAP. The effects of quartz have been linked to phagosomal destabilization (Hornung et al., 2008) and it would seem possible that the short fiber shape of the tube affects the lysosomes in a similar way (Køber et al., 2015). The materials in this study definitely end up in lysosome/phagosome structures of macrophages as seen in the EM pictures. We have previously observed PAP in rats i.t.-exposed to a short CNT (NM-403) of similar dimensions as the TiO_2 tube (Gate et al., 2019).

Prolonged pulmonary effects 28-day post exposure have been shown for various CNTs (Poulsen et al., 2013; Poulsen et al., 2015b; Poulsen et al., 2016; Poulsen et al., 2017), in addition to long retention time in the lungs 28 and 90 days post-exposure (Poulsen et al., 2016a). We recently detected MWCNTs in the lungs of mice one year after a single exposure to 54 μg MWCNT by i.t. instillation suggesting that MWCNTs are biopersistent (Knudsen et al., 2019) as also concluded in review of CNT biodistribution (Jacobsen et al., 2017). Previous mice studies have shown dose-dependent deposition and sustained retention of TiO_2 in the lungs over 28 days (Husain et al., 2013) as well as in the liver 180 day after i.t exposure (Modrzynska et al., 2018a; Modrzynska et al., 2018b). Whether the long-lasting inflammation is due to a longer retention time is unclear, but all four anatase TiO_2 NMs were still present in lungs 180 days post exposure. However, it is not possible to apply a quantitative approach, as it would require a very accurate sectioning to compare the exact same lung region across the samples.

The crystal phase of TiO_2 has been suggested to be important for the toxicological response, where rutile TiO_2 has been considered as an inert form, whereas anatase has been considered as a more active form of TiO_2 (Johnston et al., 2009). Our results show that rutile TiO_2 NMs induces a higher inflammatory response, in terms of neutrophil influx, than similar surface area doses of anatase TiO_2 NMs. A review of in vitro and in vivo TiO_2 toxicity studies concluded that anatase TiO_2 NMs generally were more toxic in terms of cytotoxicity, cell damage, ROS production and inflammation than rutile TiO_2 NMs (Johnston et al., 2009). This was based on relatively few studies investigating the importance of crystallinity. In contrast, a recent toxicogenomic study demonstrated that the overall inflammatory and transcriptional response of mice exposed to anatase TiO_2 NMs was less compared with rutile TiO_2 NMs (Rahman et al., 2017). However, the underlying mechanisms of the different responses related to crystalline structure are unknown.

In the present study, neutrophil influx correlated closely with surface area dose for both anatase (excluding the TiO_2 tube) and rutile TiO_2 NMs, but rutile showed 3.2-fold more neutrophil influx by surface area. CB has been included in our animal studies, as an internal reference particle, to allow comparison of results across studies. CB (162 μg/mouse) used in the previous studies on rutile TiO_2 NMs resulted in similar levels of neutrophil influx as observed in the present study on anatase TiO_2 NM, despite differences in vehicle composition. We are therefore confident in doing such comparisons. We have previously reported dose-dependent neutrophil influx that correlate with BET surface area of both fine and nano-sized TiO_2 and CB (Saber et al., 2018; Saber et al., 2012b). A recent paper retrospectively analyzed animal data from mice and rats on the pulmonary toxicity of i.t. instilled NMs and concluded that the BET surface area was the biologically most effective dose metric for acute pulmonary inflammation and that so-called low solubility, low toxicity (LSLT) NMs have an equivalent 30% PMN (neutrophil) influx dose range of 175 [85–405] cm^2/g lung (Schmid and Stoeger, 2016). Consequently, the neutrophil data presented here indicate that both CB as well as rutile and anatase TiO_2 NMs belong to the LSLT class of NMs.

The inflammatory response of the TiO_2 tube clearly clusters more

with rutile than anatase TiO_2 NMs, suggesting that the tube shape is a driver for the effect. In addition, the effect of BET surface area disappeared when the tube was included as a variable in the multiple regression analysis. In light of the substantial evidence for surface area being a strong predictor of inflammation for TiO_2 and carbonaceous NMs (Stoeger et al., 2007), this may indicate that the current data set has too limited variation in specific surface area (74–97 m^2/g), with the TiO_2 tube as the only anatase NM with a substantially larger BET surface area (154 m^2/g), and thus, more studies are needed to clarify this. However, both a previous (Rahman et al., 2017) and the present study suggest that in general anatase induces less inflammation than rutile NMs when normalized to surface area, however outliers like TiO_2 tube, which do not fit into the crystallinity paradigm, are possible.

In conclusion, anatase TiO_2 NMs with varying physicochemical properties induced pulmonary inflammation and pulmonary acute phase response, but no genotoxicity in mice after i.t. exposure. All four anatase TiO_2 NMs induced similar inflammatory responses when surface area was used as dose metrics, although inflammatory and acute phase response was greatest and more persistent for the TiO_2 tube. Lowest response was observed for the TiO_2 cube, which might be due to the formation of large aggregates in the lungs. Histopathological changes were observed for both TiO_2 tube and DQ12 and interestingly the effect of the TiO_2 tube was more similar to DQ12 than the other anatase TiO_2 NMs in terms of persistence and the ability to cause PAP, indicating a qualitative difference related to the tube shape. Comparison with previously published data on rutile TiO_2 NMs indicated that the rutile TiO_2 NMs were more inflammogenic in terms of neutrophil influx than anatase TiO_2 NMs when normalized to total deposited surface area. BET surface area strongly correlated with neutrophil influx for both crystal phases. Multiple regression analyses indicated that BET surface area, crystalline structure and tube shape are potentially important predictors for pulmonary inflammation and acute phase response. Overall, the results suggest that specific surface area, crystal phase and shape of TiO_2 NMs are important predictors for the observed pulmonary effects of TiO_2 NMs.

Funding

This work was supported by the European Union's Horizon 2020 research and innovation programme under Grant No. 686098 (SmartNanoTox) and the Danish Centre for Nanosafety II.

Authors' contribution

UV and KBK designed the study. KBK collected the in vivo data. JS, PU, TK and MG synthesized TiO_2 tube and TiO_2 cube and performed physicochemical characterization of the particles (TEM, XRD). HW, EV and SS analyzed and interpreted the histopathology data (light and electron microscopy). TB analyzed and interpreted the histopathology and particle distribution (light and enhanced darkfield microscopy). AMM did the endotoxin measurements. NRJ and IKW did the acellular ROS measurements. SSP performed the multiple regression analyses. PHD, KBK, UV, HW, OS and YD analyzed and interpret the data. PHD drafted the manuscript. All authors contributed to the writing of the manuscript. All authors read and approved the final manuscript.

Declaration of Competing Interest

All authors declare no competing interest.

Acknowledgements

Craig Poland is thanked for providing the benchmark particle DQ12. The technical assistance from Michael Guldbrandsen, Eva Terrida, Dorte Larsen, Anne-Karin Asp, Anne Abildtrup, Noor Irmam, Yasmin Akhtar and Margit Wagtberg Frederiksen is gratefully acknowledged.

Appendix A. Supplementary data

Supplementary data to this article can be found online at https://doi.org/10.1016/j.taap.2019.114830.

References

Baisch, B.L., Corson, N.M., Wade-Mercer, P., Gelein, R., Kennell, A.J., Oberdorster, G., Elder, A., 2014. Equivalent titanium dioxide nanoparticle deposition by intratracheal instillation and whole body inhalation: the effect of dose rate on acute respiratory tract inflammation. Part Fibre Toxicol. 11, 5.

Barfod, K.K., Bendtsen, K.M., Berthing, T., Koivisto, A.J., Poulsen, S.S., Segal, E., Verleysen, E., Mast, J., Holländer, A., Jensen, K.A., Hougaard, K.S., Vogel, U., 2020. Increased surface area of halloysite nanotubes due to surface modification predicts lung inflammation and acute phase response after pulmonary exposure in mice. Environ. Toxicol. Pharmacol. 73. https://doi.org/10.1016/j.etap.2019.103266.

Bengtson, S., Kling, K., Madsen, A.M., Noergaard, A.W., Jacobsen, N.R., Clausen, P.A., Alonso, B., Pesquera, A., Zurutuza, A., Ramos, R., Okuno, H., Dijon, J., Wallin, H., Vogel, U., 2016. No cytotoxicity or genotoxicity of graphene and graphene oxide in murine lung epithelial FE1 cells in vitro. Environ. Mol. Mutagen. 57, 469–482.

Borie, R., Danel, C., Debray, M.-P., Taille, C., Dombret, M.-C., Aubier, M., Epaud, R., Crestani, B., 2011. Pulmonary alveolar proteinosis. Eur. Respir. Rev. 20, 98–107.

Bourdon, J.A., Saber, A.T., Jacobsen, N.R., Jensen, K.A., Madsen, A.M., Lamson, J.S., Wallin, H., Møller, P., Loft, S., Yauk, C.L., Vogel, U.B., 2012. Carbon black nanoparticle instillation induces sustained inflammation and genotoxicity in mouse lung and liver. Part Fibre Toxicol. 9, 5.

Brown, G.M., Brown, D.M., Slight, J., Donaldson, K., 1991. Persistent biological reactivity of quartz in the lung - raised protease burden compared with a nonpathogenic mineral dust and microbial particles. Brit. J. Ind. Med. 48, 61–69.

Corrin, B., King, E., 1970. Pathogenesis of experimental pulmonary alveolar Proteinosis. Thorax 25, 230–236.

Crouch, E., Persson, A., Chang, D., Parghi, D., 1991. Surfactant protein-D - increased accumulation in silica-induced pulmonary Lipoproteinosis. Am. J. Pathol. 139, 765–776.

Donaldson, K., Murphy, F.A., Duffin, R., Poland, C.A., 2010. Asbestos, carbon nanotubes and the pleural mesothelium: a review of the hypothesis regarding the role of long fibre retention in the parietal pleura, inflammation and mesothelioma. Part Fibre Toxicol. 7, 5.

Ferin, J., Oberdorster, G., Penney, D.P., 1992. Pulmonary retention of ultrafine and fine particles in rats. Am. J. Resp. Cell Mol. 6, 535–542.

Garvas, M., Testen, A., Umek, P., Gloter, A., Koklic, T., Strancar, J., 2015. Protein Corona prevents TiO2 Phototoxicity. PLoS One 10, e0129577.

Gate, L., Knudsen, K.B., Seidel, C., Berthing, T., Chezeau, L., Jacobsen, N.R., Valentino, S., Wallin, H., Bau, S., Wolff, H., Sebillaud, S., Lorcin, M., Grossmann, S., Viton, S., Nunge, H., Darne, C., Vogel, U., Cosnier, F., 2019. Pulmonary toxicity of two different multi-walled carbon nanotube in rat: comparison between intratracheal instillation and inhalation. Toxicol. Appl. Pharmacol. 375, 17–31.

Gomez, V., Levin, M., Saber, A.T., Irusta, S., Dal Maso, M., Hanoi, R., Santamaria, J., Jensen, K.A., Wallin, H., Koponen, I.K., 2014. Comparison of dust release from epoxy and paint nanocomposites and conventional products during sanding and sawing. Ann. Occup. Hyg. 58, 983–994.

Hadrup, N., Bengtson, S., Jacobsen, N.R., Jackson, P., Nocun, M., Saber, A.T., Jensen, K.A., Wallin, H., Vogel, U., 2017. Influence of dispersion medium on nanomaterial-induced pulmonary inflammation and DNA strand breaks: investigation of carbon black, carbon nanotubes and three titanium dioxide nanoparticles. Mutagenesis 32, 581–597.

Hadrup, N., Rahmani, F., Jacobsen, N.R., Saber, A.T., Jackson, P., Bengtson, S., Williams, A., Wallin, H., Halappanavar, S., Vogel, U., 2019a. Acute phase response and inflammation following pulmonary exposure to low doses of zinc oxide nanoparticles in mice. Nanotoxicology 13, 1272–1292.

Hadrup, N., Knudsen, K.B., Berthing, T., Wolff, H., Bengtson, S., Kofoed, C., Espersen, R., Højgaard, C., Winther, J.R., Willemoës, M., Wedin, I., Nuopponen, M., Alenius, H., Norppa, H., Wallin, H., Vogel, U., 2019b. Pulmonaty effects of nanofibrillated celluloses in mice suggests that carboxylation lowers the inflammatory and acute phase responses. Environ. Toxicol. Pharmacol. 66, 116–125.

Halappanavar, S., Jackson, P., Williams, A., Jensen, K.A., Hougaard, K.S., Vogel, U., Yauk, C.L., Wallin, H., 2011. Pulmonary response to surface-coated nanotitanium dioxide particles includes induction of acute phase response genes, inflammatory cascades, and changes in MicroRNAs: a Toxicogenomic study. Environ. Mol. Mutagen. 52, 425–439.

Halappanavar, S., Saber, A.T., Decan, N., Jensen, K.A., Wu, D., Jacobsen, N.R., Guo, C., Rogowski, J., Koponen, I.K., Levin, M., Madsen, A.M., Atluri, R., Snitka, V., Birkedal, R.K., Rickerby, D., Williams, A., Wallin, H., Yauk, C.L., Vogel, U., 2015. Transcriptional profiling identifies physicochemical properties of nanomaterials that are determinants of the in vivo pulmonary response. Environ. Mol. Mutagen. 56, 245–264.

Heinrich, U., Fuhst, R., Rittinghausen, S., Creutzenberg, O., Bellmann, B., Koch, W., Levsen, K., 1995. Chronic inhalation exposure of Wistar rats and 2 different strains of mice to diesel-engine exhaust, carbon-black, and titanium-dioxide. Inhal. Toxicol. 7, 533–556.

Hornung, V., Bauernfeind, F., Halle, A., Samstad, E.O., Kono, H., Rock, K.L., Fitzgerald, K.A., Latz, E., 2008. Silica crystals and aluminum salts activate the NALP3 inflammasome through phagosomal destabilization. Nat. Immunol. 9, 847–856.

Husain, M., Saber, A.T., Guo, C., Jacobsen, N.R., Jensen, K.A., Yauk, C.L., Williams, A.,

Vogel, U., Wallin, H., Halappanavar, S., 2013. Pulmonary instillation of low doses of titanium dioxide nanoparticles in mice leads to particle retention and gene expression changes in the absence of inflammation. Toxicol. Appl. Pharmacol. 269, 250–262.
IARC, 2010. Carbon Black, Titanium Dioxide, and Talc. IARC Monographs on the Evaluation of Carcinogenic Risks to Humans. WHO, The International Agency for Research on Cancer, Lyon, pp. 93.
Jackson, P., Lund, S.P., Kristiansen, G., Andersen, O., Vogel, U., Walin, H., Hougaard, K.S., 2010. An experimental protocol for maternal pulmonary exposure in developmental toxicology. Basic. Clin. Pharmacol. 108, 202–207.
Jackson, P., Halappanavar, S., Hougaard, K.S., Williams, A., Madsen, A.M., Lamson, J.S., Andersen, O., Yauk, C., Wallin, H., Vogel, U., 2013a. Maternal inhalation of surface-coated nanosized titanium dioxide (UV-titan) in C57BL/6 mice: effects in prenatally exposed offspring on hepatic DNA damage and gene expression. Nanotoxicology 7, 85–96.
Jackson, P., Pedersen, L.M., Kyjovska, Z.O., Jacobsen, N.R., Saber, A.T., Hougaard, K.S., Vogel, U., Wallin, H., 2013b. Validation of freezing tissues and cells for analysis of DNA strand break levels by comet assay. Mutagenesis 28, 699–707.
Jacobsen, N.R., Pojana, G., White, P., Møller, P., Cohn, C.A., Korsholm, K.S., Vogel, U., Marcomini, A., Loft, S., Wallin, H., 2008. Genotoxicity, cytotoxicity, and reactive oxygen species induced by single-walled carbon nanotubes and C(60) fullerenes in the FE1-Mutatrade markMouse lung epithelial cells. Environ. Mol. Mutagen. 49, 476–487.
Jacobsen, N.R., Møller, P., Jensen, K.A., Vogel, U., Ladefoged, O., Loft, S., Wallin, H., 2009. Lung inflammation and genotoxicity following pulmonary exposure to nanoparticles in ApoE(−/−) mice. Part Fibre Toxicol. 6, 2.
Jacobsen, N.R., Møller, P., Clausen, P.A., Saber, A.T., Micheletti, C., Jensen, K.A., Wallin, H., Vogel, U., 2017. Biodistribution of carbon nanotubes in animal models. Basic Clin. Pharmacol. 121, 30–43.
Johnston, H.J., Hutchison, G.R., Christensen, F.M., Peters, S., Hankin, S., Stone, V., 2009. Identification of the mechanisms that drive the toxicity of TiO_2 particulates: the contribution of physicochemical characteristics. Part Fibre Toxicol. 6, 33.
Kermanizadeh, A., Pojana, G., Gaiser, B.K., Birkedal, R., Bilanicova, D., Wallin, H., Jensen, K.A., Sellergren, B., Hutchison, G.R., Marcomini, A., Stone, V., 2013. In vitro assessment of engineered nanomaterials using a hepatocyte cell line: cytotoxicity, pro-inflammatory cytokines and functional markers. Nanotoxicology 7, 301–313.
Knudsen, K.B., Berthing, T., Jackson, P., Poulsen, S.S., Mortensen, A., Jacobsen, N.R., Skaug, V., Szarek, J., Hougaard, K.S., Wolff, H., Wallin, H., Vogel, U., 2019. Physicochemical predictors of multi-walled carbon nanotube-induced pulmonary histopathology and toxicity one year after pulmonary deposition of 11 different multi-walled carbon nanotubes in mice. Basic Clin. Pharmacol. 124, 211–227.
Køhler, C., Poulsen, S.S., Saber, A.T., Jacobsen, N.R., Wallin, H., Yauk, C.L., Halappanavar, S., Vogel, U., Qvortrup, K., Mølhave, K., 2015. Time-dependent subcellular distribution and effect of carbon nanotubes in lungs of mice. PLoS One 10, e0116481.
Lee, K.P., Trochimowicz, H.J., Reinhardt, C.F., 1985. Pulmonary response of rats exposed to titanium dioxide (TiO2) by inhalation for two years. Toxicol. Appl. Pharmacol. 79, 179–192.
Mikkelsen, L., Sheykhzade, M., Jensen, K.A., Saber, A.T., Jacobsen, N.R., Vogel, U., Wallin, H., Loft, S., Møller, P., 2011. Modest effect o plque progression and vasodiltory function in atherosclerosis-prone mice exposed to nanosized TiO2. Part Fibre Toxicol. 8, 32.
Modrzynska, J., Berthing, T., Ravn-Haren, G., Jacobsen, N.R., Weydahl, I.K., Loeschner, K., Mortensen, A., Saber, A.T., Vogel, U., 2018a. Primary genotoxicity in the liver following pulmonary exposure to carbon black nanoparticles in mice. Part Fibre Toxicol. 15, 2.
Modrzynska, J., Berthing, T., Ravn-Haren, G., Kling, K., Mortensen, A., Rasmussen, R.R., Larsen, E.H., Saber, A.T., Vogel, U., 2018b. In vivo-induced size transformation of cerium oxide nanoparticles in both lung and liver does not affect long-term hepatic accumulation following pulmonary exposure. PLoS One 13.
Møller, P., Jacobsen, N.R., Folkmann, J.K., Danielsen, P.H., Mikkelsen, L., Hemmingsen, J.G., Vesterdal, L.K., Forchhammer, L., Wallin, H., Loft, S., 2010. Role of oxidative damage in toxicity of particulates. Free Radic. Res. 44, 1–46.
Møller, P., Jensen, D.M., Wils, R.S., Andersen, M.H.G., Danielsen, P.H., Roursgaard, M., 2017. Assessment of evidence for nanosized titanium dioxide-generated DNA strand breaks and oxidatively damaged DNA in cells and animal models. Nanotoxicology 11, 1237–1256.
Poulsen, S.S., Jacobsen, N.R., Labib, S., Wu, D., Husain, M., Williams, A., Bøgelund, J.P., Andersen, O., Køhler, C., Mølhave, K., Kyjovska, Z.O., Saber, A.T., Wallin, H., Yauk, C.L., Vogel, U., Halappanavar, S., 2013. Transcriptomic analysis reveals novel mechanistic insight into murine biological responses to multi-walled carbon nanotubes in lungs and cultured lung epithelial cells. PLoS One 8.
Poulsen, S.S., Saber, A.T., Mortensen, A., Szarek, J., Wu, D.M., Williams, A., Andersen, O., Jacobsen, N.R., Yauk, C.L., Wallin, H., Halappanavar, S., Vogel, U., 2015a. Changes in cholesterol homeostasis and acute phase response link pulmonary exposure to multi-walled carbon nanotubes to risk of cardiovascular disease. Toxicol. Appl. Pharmacol. 283, 210–222.
Poulsen, S.S., Saber, A.T., Williams, A., Andersen, O., Kobler, C., Atluri, R., Pozzebon, M.E., Mucelli, S.P., Simion, M., Rickerby, D., Mortensen, A., Jackson, P., Kyjovska, Z.O., Mølhave, K., Jacobsen, N.R., Jensen, K.A., Yauk, C.L., Wallin, H., Halappanavar, S., Vogel, U., 2015b. MWCNTs of different physicochemical properties cause similar inflammatory responses, but differences in transcriptional and histological markers of fibrosis in mouse lungs. Toxicol. Appl. Pharmacol. 284, 16–32.
Poulsen, S.S., Jackson, P., Kling, K., Knudsen, K.B., Skaug, V., Kyjovska, Z.O., Thomsen, B.L., Clausen, P.A., Atluri, R., Berthing, T., Bengtson, S., Wolff, H., Jensen, K.A., Wallin, H., Vogel, U., 2016. Multi-walled carbon nanotube physicochemical properties predict pulmonary inflammation and genotoxicity. Nanotoxicology 10, 1263–1275.
Poulsen, S.S., Knudsen, K.B., Jackson, P., Weydahl, I.E., Saber, A.T., Wallin, H., Vogel, U., 2017. Multi-walled carbon nanotube-physicochemical properties predict the systemic acute phase response following pulmonary exposure in mice. PLoS One 12, e0174167.
Rahman, L., Wu, D., Johnston, M., Williams, A., Halappanavar, S., 2017. Toxicogenomics analysis of mouse lung responses following exposure to titanium dioxide nanomaterials reveal their disease potential at high doses. Mutagenesis 32, 59–76.
Saber, A.T., Halappanavar, S., Folkmann, J.K., Bornholdt, J., Boisen, A.M., Møller, P., Williams, A., Yauk, C., Vogel, U., Loft, S., Wallin, H., 2009. Lack of acute phase response in the livers of mice exposed to diesel exhaust particles or carbon black by inhalation. Part Fibre Toxicol. 6, 12.
Saber, A.T., Jacobsen, N.R., Mortensen, A., Szarek, J., Jackson, P., Madsen, A.M., Jensen, K.A., Koponen, I.K., Brunborg, G., Gutzkow, K.B., Vogel, U., Wallin, H., 2012a. Nanotitanium dioxide toxicity in mouse lung is reduced in sanding dust from paint. Part Fibre Toxicol. 9, 4.
Saber, A.T., Jensen, K.A., Jacobsen, N.R., Birkedal, R., Mikkelsen, L., Møller, P., Loft, S., Wallin, H., Vogel, U., 2012b. Inflammatory and genotoxic effects of nanoparticles designed for inclusion in paints and lacquers. Nanotoxicology 6, 453–471.
Saber, A.T., Lamson, J.S., Jacobsen, N.R., Ravn-Haren, G., Hougaard, K.S., Nyendi, A.N., Wahlberg, P., Madsen, A.M., Jackson, P., Wallin, H., Vogel, U., 2013. Particle-induced pulmonary acute phase response correlates with neutrophil influx linking inhaled particles and cardiovascular risk. PLoS One 8, e69020.
Saber, A.T., Jacobsen, N.R., Jackson, P., Poulsen, S.S., Kyjovska, Z.O., Halappanavar, S., Yauk, C.L., Wallin, H., Vogel, U., 2014. Particle-induced pulmonary acute phase response may be the causal link between particle inhalation and cardiovascular disease. Wiley Interdiscip. Rev. Nanomed. Nanobiotechnol. 6, 517–531.
Saber, A.T., Mortensen, A., Szarek, J., Jacobsen, N.R., Levin, M., Koponen, I.K., Jensen, K.A., Vogel, U., Wallin, H., 2018. Toxicity of pristines and paint-embedded TiO2 nanomaterials. Human and Experimental Toxicology 1–14.
Saber, A.T., Mortensen, A., Szarek, J., Koponen, I.K., Levin, M., Jacobsen, N.R., Pozzebon, M.E., Mucelli, S.P., Rickerby, D.G., Kling, K., Atluri, R., Madsen, A.M., Jackson, P., Kyjovska, Z.O., Vogel, U., Jensen, K.A., Wallin, H., 2016. Epoxy composite dusts with and without carbon nanotubes cause similar pulmonary responses, but differences in liver histology in mice following pulmonary deposition. Part Fibre Toxicol. 13, 37.
Schmid, O., Stoeger, T., 2016. Surface area is the biologically most effective dose metric for acute nanoparticle toxicity in the lung. J. Aerosol Sci. 99, 133–143.
Seymour, J.F., Presneill, J.J., 2002. Pulmonary alveolar proteinosis - Progress in the first 44 years. Am J Resp Crit Care 166, 215–235.
Shi, H.B., Magaye, R., Castranova, V., Zhao, J.S., 2013. Titanium dioxide nanoparticles: a review of current toxicological data. Part Fibre Toxicol. 10, 15.
Stoeger, T., Schmid, O., Takenaka, S., Schulz, H., 2007. Inflammatory response to TiO2 and carbonaceous particles scales best with BET surface area. Environ. Health Perspect. 115, A290–A291 author reply. A291–292.
Stone, V., Miller, M.R., Clift, M.J.D., Elder, A., Mills, N.L., Møller, P., Schins, R.P.F., Vogel, U., Kreyling, W.G., Jensen, K.A., Kuhlbusch, T.A.J., Schwarze, P.E., Hoet, P., Pietroiusti, A., De Vizcaya-Ruiz, A., Baeza-Squiban, A., Teixeira, J.P., Tran, C.L., Cassee, F.R., 2017. Nanomaterials versus ambient ultrafine particles: an opportunity to exchange toxicology knowledge. Environ. Health Perspect. 125.
Urbancic, I., Garvas, M., Kokot, B., Majaron, H., Umek, P., Cassidy, H., Skarabot, M., Schneider, F., Galiani, S., Arsov, Z., Koklic, T., Matallanas, D., Ceh, M., Musevic, I., Eggeling, C., Strancar, J., 2018. Nanoparticles can wrap epithelial cell membranes and relocate them across the epithelial cell layer. Nano Lett. 18, 5294–5305.
Wallin, H., Kyjovska, Z.O., Poulsen, S.S., Jacobsen, N.R., Saber, A.T., Bengtson, S., Jackson, P., Vogel, U., 2017. Surface modification does not influence the genotoxic and inflammatory effects of TiO2 nanoparticles after pulmonary exposure by instillation in mice. Mutagenesis 32, 47–57.
Warheit, D.B., Brock, W.J., Lee, K.P., Webb, T.R., Reed, K.L., 2005. Comparative pulmonary toxicity inhalation and instillation studies with different TiO2 particles formulations: Impact of surface treatments on particle toxicity. Toxicological Sciences 88, 514–524.
Yang, L., Feuchtinger, A., Moller, W., Ding, Y., Kutschke, D., Moller, G., Schittny, J.C., Burgstaller, G., Hofmann, W., Stoeger, T., Daniel, R., Walch, A., Schmid, O., 2019. Three-Dimentional quantitative co-mapping of pulmonary morphology and nanoparticle distribution with cellular resolution in nondissected murine lungs. ACS Nano 13, 1029–1041.